RESEARCH ARTICLE SUMMARY

BLOOD STEM CELLS

Transcripts of repetitive DNA elements signal to block phagocytosis of hematopoietic stem cells

Cecilia Pessoa Rodrigues, Joseph M. Collins, Song Yang, Catherine Martinez, Ji Wook Kim, Chhiring Lama, Anna S. Nam, Clemens Alt, Charles Lin, Leonard I. Zon*

INTRODUCTION: Hematopoietic stem and progenitor cells (HSPCs) produce mature blood cells throughout life. During this process, HSPCs engage in interactions with the variety of cells present in the marrow niche, including macrophages. These macrophages mediate a myriad of processes by releasing cytokines and chemokines and patrolling to remove stressed, dead, or aging cells. In this manner, macrophages contribute to the maintenance of tissue homeostasis. During hematopoiesis, macrophages ensure the quality of normal blood stem cells and determine the number of hematopoietic clones that participate in adult hematopoiesis. They then either engulf a stem cell completely, referred to as "dooming," or capture portions of the stem cell's cellular material, referred to as "grooming." After grooming, the stem cell continues to divide, whereas the doomed HSPC clone is eliminated.

RATIONALE: Past work has shown that the HSPC-macrophage interaction is mediated by an "eat-me" signal, calreticulin (Calr), on the surface of HSPCs. Surface Calr levels are increased in stem cells with higher levels of reactive oxygen species (ROS), and this triggers macrophages to engulf and kill stem cells that have high amounts of stress-activated proteins. However, the specific molecular cues that regulate the dooming versus grooming behavior are still unknown.

RESULTS: To investigate the cues mediating grooming versus dooming, we screened a panel of 1200 bioactive small molecules in human cells and identified 93 compounds that robustly increased surface CALR in a dose-dependent manner. Of these compounds, 22 also facilitated interactions between macrophages and stem cells in zebrafish. Compounds that depended on ROS to increase CALR showed higher dooming ratios and, conversely, animals treated with ROS-independent compounds exhibited a higher probability of grooming events despite increased CALR and increased macrophage–stem cell interactions. To investigate the signals involved in interactions under ROS-independent conditions, we undertook a genome-wide screen in human cells. We identified Toll-like receptor 3 (TLR3) as a CALR inducer in the "don't eat me" context. Next, we found that TLR3 expression was required for the expression of the "don't eat me" signal Beta-2-microglobulin (*B2M*). Antibody staining and studies of a *b2m* knockout zebrafish line showed that b2m on stem cells was required for preventing the macrophage dooming. To determine whether the increased dooming observed in the *b2m* mutant affected clonal dominance, we generated mosaic deletions using the zebrabow color barcoding system (TWISTR) as a lineage tracer. Mosaic deletion of *b2m* reduced the number of myeloid clones but increased clonal dominance. The dominant clones in these fish were wild type for *b2m* that were resistant to dooming and overtook the adult marrow. TLR3 signaling is activated by double-stranded RNA, which can sometimes be found in cells due to the expression of transcripts associated with repetitive elements (REs), including long terminal repeats (LTRs) and endogenous retroviruses. RE expression in HSPCs positively correlated with elevated levels of B2m. Moreover, overexpressing ltr4 in zebrafish led to higher HSPC proliferation, indicative of decreased dooming. Impairing the TLR3-B2M pathway by disrupting the expression of TLR3, IRF3, or B2M expression decreased the number of blood cell clones in zebrafish. Using the DNA methyltransferase inhibitor CM272 to promote upregulation of REs amplified the proliferation of already established HSPC clones in zebrafish embryos.

CONCLUSION: Our findings support a model in which endogenous TLR3 ligands lead to expression of b2m, thereby providing a blockade against macrophage-induced dooming and determining hematopoietic stem cell clonality by monitoring stem cell quality with macrophages. The balance of Calr and B2m governs the number of long-lived HSC clones that contribute to the adult blood system through macrophage-mediated quality assurance. This sheds light on the intricate interplay between HSPC clonal expansion and immune-regulated cell clearance. We propose that this protective mechanism may also operate in adulthood in response to environmental stress, such as during infections or in clonal stem cell disorders. Manipulating the levels of "don't eat-me" and "eat-me" signals may have important therapeutic implications for immune therapy by harnessing the macrophage-selective removal of a mutated stem cell clone. ■

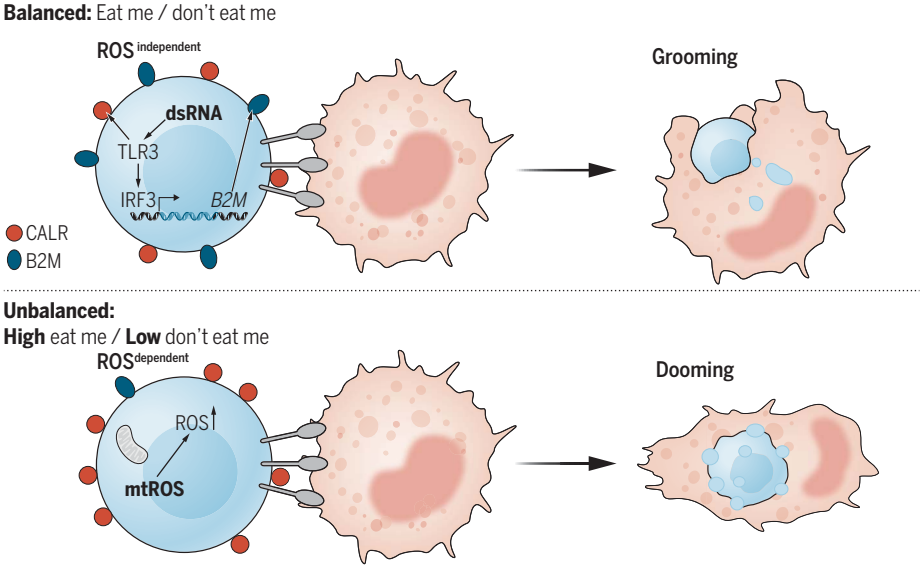

ROS and TLR3 signaling mediates the "eat-me" and "don't eat me" signals that determine stem cell clonal selection by macrophages. Shown is a schematic overview of the proposed model showing the balance between the Calr-mediated "eat-me" and B2m-mediated "don't eat-me" signals that influence macrophage behavior.

The list of author affiliations is available in the full article online.
*Corresponding author. Email: zon@enders.tch.harvard.edu
Cite this article as C. Pessoa Rodrigues *et al.*, *Science* **385**, eadn1629 (2024). DOI: 10.1126/science.eadn1629

READ THE FULL ARTICLE AT
https://doi.org/10.1126/science.adn1629

RESEARCH ARTICLE

BLOOD STEM CELLS

Transcripts of repetitive DNA elements signal to block phagocytosis of hematopoietic stem cells

Cecilia Pessoa Rodrigues[1,2], Joseph M. Collins[1,2], Song Yang[1], Catherine Martinez[2], Ji Wook Kim[1,2], Chhiring Lama[3], Anna S. Nam[3], Clemens Alt[4], Charles Lin[4,5], Leonard I. Zon[1,2]*

Macrophages maintain hematopoietic stem cell (HSC) quality by assessing cell surface Calreticulin (Calr), an "eat-me" signal induced by reactive oxygen species (ROS). Using zebrafish genetics, we identified Beta-2-microglobulin (B2m) as a crucial "don't eat-me" signal on blood stem cells. A chemical screen revealed inducers of surface Calr that promoted HSC proliferation without triggering ROS or macrophage clearance. Whole-genome CRISPR-Cas9 screening showed that Toll-like receptor 3 (Tlr3) signaling regulated *b2m* expression. Targeting *b2m* or *tlr3* reduced the HSC clonality. Elevated B2m levels correlated with high expression of repetitive element (RE) transcripts. Overall, our data suggest that RE-associated double-stranded RNA could interact with TLR3 to stimulate surface expression of B2m on hematopoietic stem and progenitor cells. These findings suggest that the balance of Calr and B2m regulates macrophage-HSC interactions and defines hematopoietic clonality.

Development, tissue integrity, and defense against immunogenic challenges necessitate the effective removal of damaged and impaired cells (*1*, *2*). Innate immune cells such as macrophages and neutrophils orchestrate the removal or phagocytosis of these dying cells by discriminating between molecules expressed on their surfaces (*2*). Therefore, the phagocytic process needs to be carefully regulated to avoid the unwarranted elimination of healthy cells (*2*). Surface molecules such as complement, opsonins, exposed phosphatidylserine (PS), Calreticulin (Calr), and annexin I serve as signals to initiate the phagocytosis ("eat-me") signal (*2*). These surface molecules are not present at high levels on the surfaces of living healthy cells except during specific physiological events. By contrast, surface molecules such as Beta-2-microglobulin (B2m) serve as "don't eat-me" signals to prevent the unwarranted clearance of healthy cells that concurrently present eat-me molecules on their surfaces (*3*, *4*).

Hematopoietic stem cells (HSCs) that originate during embryonic development sustain lifelong tissue homeostasis (*5*) and phagocytosis by macrophages plays a pivotal role in ensuring the quality of newly formed hematopoietic stem and progenitor cells (HSPCs) within the embryonic niche (*6*).

[1]Howard Hughes Medical Institute, Boston Children's Hospital Boston, MA, USA. [2]Harvard Stem Cell Institute, Stem Cell and Regenerative Biology Department, Harvard University, Cambridge, MA, USA. [3]Department of Pathology and Laboratory Medicine, Weill Cornell Medicine, New York, NY, USA. [4]Wellman Center for Photomedicine, Mass General Research Institute, Boston, MA, USA. [5]Center for Systems Biology, Massachusetts General Hospital, Boston, MA, USA.
*Corresponding author. Email: zon@enders.tch.harvard.edu

HSPCs present surface Calr as an "eat-me" signal that induces macrophage interaction. During their interaction, a macrophage may completely engulf an HSPC (dooming) or sample a small portion of the HSPC cellular material without killing it (grooming) (*6*). Whereas HSPC dooming eliminates a selected stem cell clone, HSPC grooming likely regulates HSPC proliferation by activating interleukin 1β (Il-1β)–dependent signaling (*6*). Grooming and dooming are important quality control steps that remove stressed HSPCs during development. Despite the importance of these processes, the mechanism by which macrophages distinguish which HSPCs to doom and which HSPCs to groom remains elusive. Through live imaging and in vivo cellular barcoding techniques, we demonstrate here that the balance between "eat-me" and "don't eat-me" signals is provided by reactive oxygen species (ROS) and toll-like receptor 3 (Tlr3) activation, respectively. These signals determine the number of long-lived HSC clones that contribute to the adult blood system through macrophage-mediated quality assurance mechanisms.

Results

Calr expression is induced by processes associated with and without ROS

Stress associated with ROS within HSPCs mediates the surface presentation of "eat-me" molecules as Calr (*6*). This stress in HSPCs correlates with FoxO signaling, which is known to mediate cellular detoxification from spurious ROS (*7*). Similar to the proposed quality control mechanism, we observed that HSPCs with high ROS were removed (doomed) by macrophages, whereas low ROS HSPCs were not doomed, but rather prompted to continue dividing after interacting with macrophages (Fig. 1A and movie S1). We evaluated ROS levels in zebrafish HSPCs and confirmed that increased levels of ROS correlated with surface presentation of the "eat-me" signal, Calr (Fig. 1B and fig. S1A). Conversely, when we reduced ROS in HSPCs by treating zebrafish embryos with the ROS scavengers diphenyleneiodonium (DPI) and VAS2870 (VAS) (*8*), we observed low levels of surface Calr (Fig. 1C) and reduced macrophage interactions (*6*) with stem cells. This shows that ROS levels are indicative of higher surface Calr and presumably a macrophage-HSPC interaction.

Nonetheless, the intrinsic mechanism regulating surface Calr in a ROS-independent manner remains unknown. To systematically evaluate the pathways in HSPCs that trigger surface Calr presentation, we targeted a myriad of signaling pathways in human embryonic kidney 293 (HEK293) cells by screening a panel of 1200 bioactive small molecules (Fig. 1D). Calr is an abundant chaperone in the endoplasmic reticulum (ER). Thus, to evaluate only Calr on the cell surface, we designed a SPLIT-TURBO ID (*9*) construct targeting the association of Calr and a membrane protein, Cadherin 2 (CDH2). We orthogonally evaluated Calr surface presentation with a fluorescent Calr antibody (Zenon-Technology). Through these two independent approaches, we identified compounds that robustly increase surface Calr presentation. Concurrently, we also labeled cells with CellROX (Thermo Fisher Scientific), a ubiquitous ROS probe, to identify compounds that induce surface Calr in a ROS-associated manner (Fig. 1D and fig. S1, B and C). We found 93 compounds that increased surface Calr with a robust dose-dependent response in cells (Fig. 1E), hereafter referred to as Calr inducers. Among the 93 Calr inducers, 54 were associated with an increase of ROS (ROS-dependent), whereas 39 did not affect ROS levels (ROS-independent) (data S1). Dimethyl sulfoxide (DMSO) was used as the vehicle control, and DPI and H_2O_2 were used as internal negative and positive controls, respectively. Using the Chemical Annotation Toolkit (*10*), we analyzed the known biological function of ROS-dependent compounds. As expected, we found a strong positive correlation with cellular stress pathways, such as oxidation by cytochrome P450 and DNA damage, whereas ROS-independent chemicals were not enriched in a given pathway (data S1).

To test the effect of the 93 Calr inducers on macrophage-HSPC interaction outcomes, we used *runx1*$^{+}$*23:mCherry; mpeg1.1:EGFP* zebrafish embryos expressing fluorescent reporters in HSPCs and macrophages, respectively (*11*). At 48 hours postfertilization (hpf), embryos were exposed to the 93 Calr inducers (Fig. 1F). After 24 hours of exposure, we evaluated macrophage-HSPC interactions by live-cell imaging. Twenty-two of 93 Calr inducers facilitated macrophage-HSPC interactions above

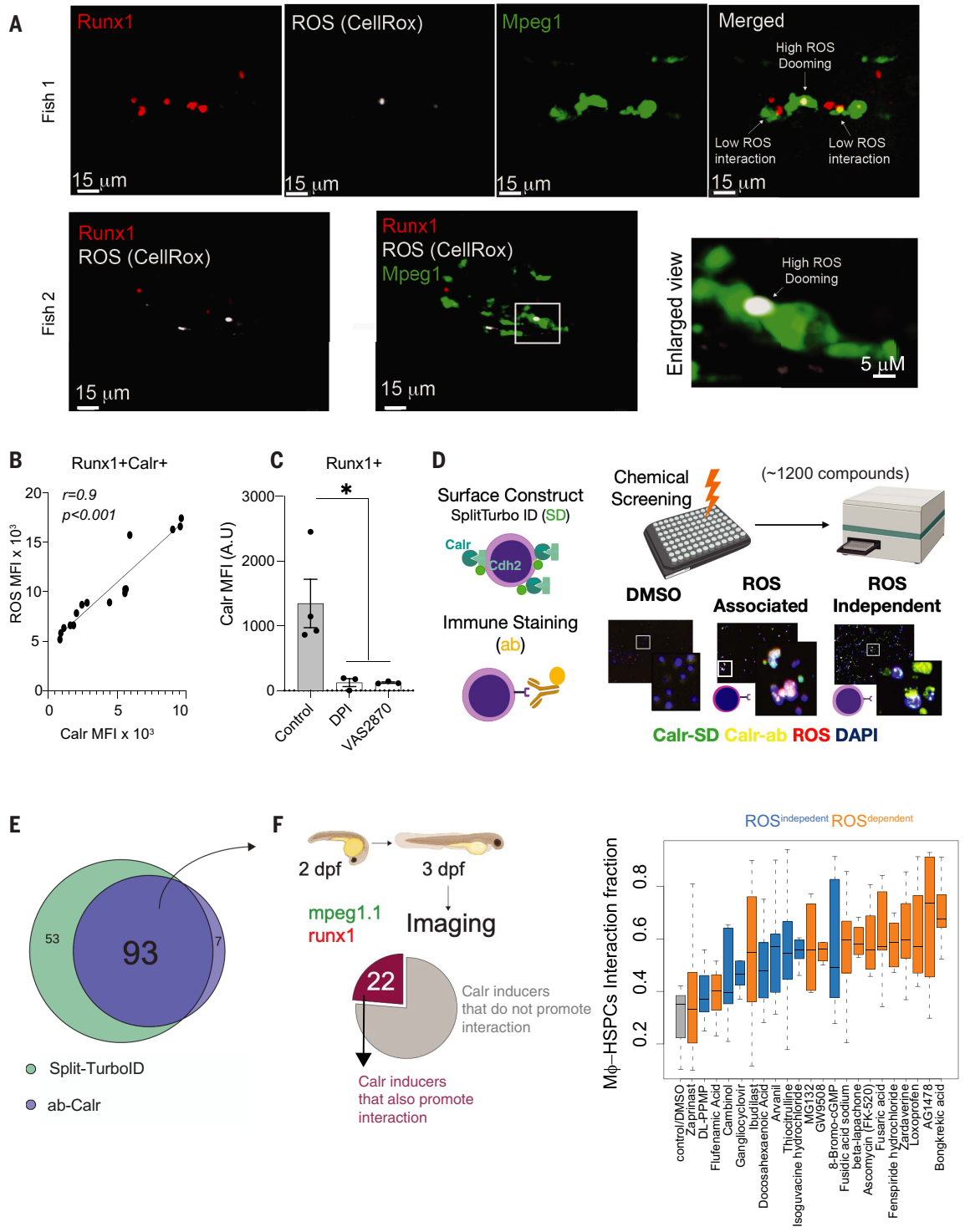

Fig. 1. Chemical screen identifies ROS-dependent and ROS-independent surface Calr inducers. (**A**) Representative imaging from three independent experiments showing that ROS^{+}Runx1^{+} cells are preferentially doomed by the macrophages. Green indicates Mpeg; red, Runx1; and white, the CellRox probe. (**B**) ROS levels in embryonic HSPCs marked by surface Calr. Data were analyzed by Pearson correlation. MFI, median fluorescence intensity; AU, arbitrary unit. Data points represent a pool of 100 to 300 3-dpf embryos (**C**) Surface Calr levels on HSPCs after ROS inhibition with DPI or VAS2870 (a Nox inhibitor). Data were analyzed by Kruskall-Wallis test followed by Dunn's test; *P < 0.05. Data points represent a pool of 100 to 300 3-dpf embryos. Data in (A) to (C) are shown as means ± SEM. Experiments were performed in a pool of 100 to 300 zebrafish embryos in two independent experiments. (**D**) Schematic overview of the chemical screen. Two approaches were used to ensure that our system specifically recorded the surface Calr values: (i) HEK293 cells were transfected with the SPLIT-TURBO ID where the C terminus was designed to carry Cdh2, a membrane protein, whereas the N terminus was carrying Calr; and (ii) anti-Calr was conjugated with a A647 using Zenon technology. Next, the cells were plated in 384-well plates and treated with a panel of 1200 bioactive small molecules in three different concentrations, 5, 2.5, and 0.625 μM. The cells were also labeled with a ubiquitous ROS

probe (CellRox) and DAPI for nuclear staining. After 24 hours, the Zeiss Cell Discoverer 7 (CR7) microscope was used to read the plates. Data were analyzed using the CellProfiler and R-Sight HTS software. SD, Split-turbo ID; ab, Calr antibody. (**E**) Numbers and overlap in compounds that induced surface Calr in HEK293 for both systems. Each compound was tested in replicates, and two to four random fields of view were chosen for acquisition. The same well was used for SPLIT-Turbo, Ab-Calr, and CellROX acquisition. (**F**) Left: number of compounds that increased surface Calr in vitro and in vivo (zebrafish embryos). Right: live image microscopy was used to determine the interaction fraction between macrophage-HSPCs using *mpeg-GFP;runx1-mCherry* embryos that label macrophage and HSPCs, respectively. Highlighted in blue are the ROS-independent compounds, and black represents the ROS-dependent compounds. Data are shown are means ± SEM. The zebrafish live-imaging experiments performed to determine the macrophage-HSPC interaction were conducted as two independent experiments, and a minimum of five embryos were imaged.

baseline levels (Fig. 1F and data S1). We confirmed increased surface Calr presentation by these compounds (fig. S1D).

Both ROS-dependent and ROS-independent compounds increased macrophage-HSPC interaction ratios by a similar level (fig. S1E). We evaluated apoptosis by Annexin-V staining on cells from wild-type (WT) 72 hpf embryos. The 22 compounds did not change apoptosis levels compared with DMSO-treated embryos except for the ROS-dependent β-lapachone (Fig. 1G and fig. S1F). Thus, Calr inducers triggered surface Calr independently of an apoptotic and/or cell death pathway (fig. S1, D to F). Next, to validate the dependence of Calr in mediating the increased macrophage-HSPCs interaction observed upon treatment with the 22 Calr inducers (Fig. 1G), we generated mosaic deletions (crispants) of a *Calr* isoform in zebrafish that regulates macrophage-HSPC interactions, *Calr3b* (*6*). We found that the 22 Calr inducers facilitated the interaction in a *Calr3b*-dependent manner (fig. S1, G and H). Collectively, these results demonstrate that surface Calr level determines the macrophage-HSPC interaction. Both ROS-dependent and ROS-independent pathways increase surface Calr presentation, suggesting that various sources of stress lead to the presentation of "eat-me" signals.

Macrophage dooming or grooming behavior is determined by HSPC ROS levels

Because antioxidant treatment hinders the surface Calr levels of human HSPCs exposed to ROS-dependent compounds (fig. S1I), we reasoned that compounds that promoted dooming would be associated with higher ROS levels due to mitochondrial dysfunction. Supporting our hypothesis, ROS-dependent compounds that promoted only dooming (Fig. 2A) also impaired mitochondrial membrane potential (fig. S1, J to L), and the absence of macrophage-HSPC interactions induced a higher accumulation of mitochondrial ROS (fig. S1, M and N), thus supporting quality control being ensured by macrophages.

By contrast, ROS-independent compounds increased HSPC proliferation, which was consistent with increased grooming behavior (Fig. 2A and fig. S2A). These results suggested that surface Calr presentation on HSPCs induce macrophage interaction, but also that the outcome of that interaction is determined by HSPC cellular ROS levels. ROS-dependent compounds stimulated dooming behavior and HSPC death. ROS-independent compounds stimulated grooming behavior and HSPC proliferation.

The pro-proliferative effect of Calr-inducing compounds on HSPCs could be an indirect consequence of impaired intrinsic macrophage behavior. Therefore, we tested the chemotaxis and phagocytic activity of macrophages treated with ROS-independent compounds in vitro. To evaluate phagocytosis, we treated RAW-274 macrophages with the Calr inducers. After exposure for 24 hours, we added green fluorescent protein (GFP)–rhodo zymosan, a pathogen particle that promotes phagocytosis, to the culture and measured the number of zymosan-GFP^+ macrophages by live-cell imaging. We did not observe impaired zymosan phagocytosis in the treated cells. Lipopolysaccharide (LPS) was used as a positive macrophage stimulator (fig. S2B). We evaluated macrophage chemotaxis with an agarose-chemotaxis assay (*12*). RAW-274 cells were treated with DMSO (negative control), LPS (positive control), or the ROS-independent compound. The chemoattractant spot was filled with a medium containing LPS as bait for macrophage chemotaxis, which was not affected by this treatment (fig. S2C). These results suggested that ROS-independent Calr inducers did not alter intrinsic macrophage function. Thus, ROS-independent compounds drive macrophage-mediated HSPC grooming without inducing macrophage-autonomous effects (Fig. 2A).

Tlr3 induces surface Calr in a progrooming context

To determine how ROS-independent compounds induce surface Calr presentation to promote macrophage grooming, rather than dooming, we conducted a genome-wide CRISPR screen. We chose the ROS-independent compound DL-PPMP as the Calr inducer because it led to high surface Calr (fig. S1C), macrophage-HSPC interactions (Fig. 1F), and HSPC proliferation (fig. S2A) and also increased the macrophage grooming ratio (Fig. 2A and movie S2). To define the intricate network required for surface Calr expression, we used a lentiviral delivery of a knockout library that targeted 18,080 genes with 64,751 unique guide sequences (*13*). We treated K562 human leukemia cells with DL-PPMP or DMSO (control) and sorted them using flow for $Calr^-$ cells (Fig. 2B). Here, by sorting for $Calr^-$ cells and enriching for the single-guide RNA (sgRNA) in them, we determined which genes regulate surface Calr presentation in response to the Calr inducer in the "don't eat-me" context.

We focused on the genes that were specifically enriched in the DL-PPMP–stimulated cells (Fig. 2C and data S2). Among the targets, we found enrichment of genes that up-regulate Calr presentation and are associated with cytosolic DNA/RNA sensing and viral immune responses. TLR3, a double-stranded RNA (dsRNA) sensor; DDX3X, a RNA helicase; and XBP1, a protein that, among other things, regulates major histocompatibility complex class II (MHC-II) genes and is a key transcription factor regulator of ER stress (*14*–*16*). In validation experiments, *TLR3* depletion reduced surface Calr in K562 cells (fig. S2G), indicating that cytosolic DNA and/or RNA may mediate the increase in surface Calr.

In parallel, we performed a whole-genome CRISPR-Cas9 screen of K562 cells treated with a ROS-dependent compound that promotes HSPC dooming, bongkrekic acid. Although we scored enrichment of Calr, confirming the targeting efficiency of our screen, we did not find enrichment of *TLR3* in this dataset (data S2). These data supported the hypothesis that a progrooming surface Calr presentation is mediated by TLR3.

Tlr3 signaling in HSPCs is required for macrophage-mediated grooming

We sought to evaluate the biological relevance of Tlr3 in HSPCs for controlling dooming versus grooming by macrophages. We tested this with two orthogonal approaches. We depleted *tlr3* by injecting a morpholino in single-cell zebrafish embryos ("morphants"; fig. S2H) or we pharmacologically inhibited Tlr3 by treating zebrafish embryos with the dsRNA/Tlr3 inhibitor (fig. S2I), CUCPT4a (iTlr3) (*17*). We treated or depleted 48 hours after the emergence or budding of HSPCs from the ventral wall of the dorsal aorta reliably occurred during the first 48 hpf (*18*). In both approaches, we observed a reduced number of HSPCs presenting surface Calr in vivo by flow cytometry (fig. S2, H and I). These data confirmed that Tlr3 is required for surface Calr presentation on the surface of HSPCs in vivo.

We then tested if morpholino-depletion of *tlr3* or iTlr3 inhibition modulated macrophage-HSPC interactions and interaction outcomes.

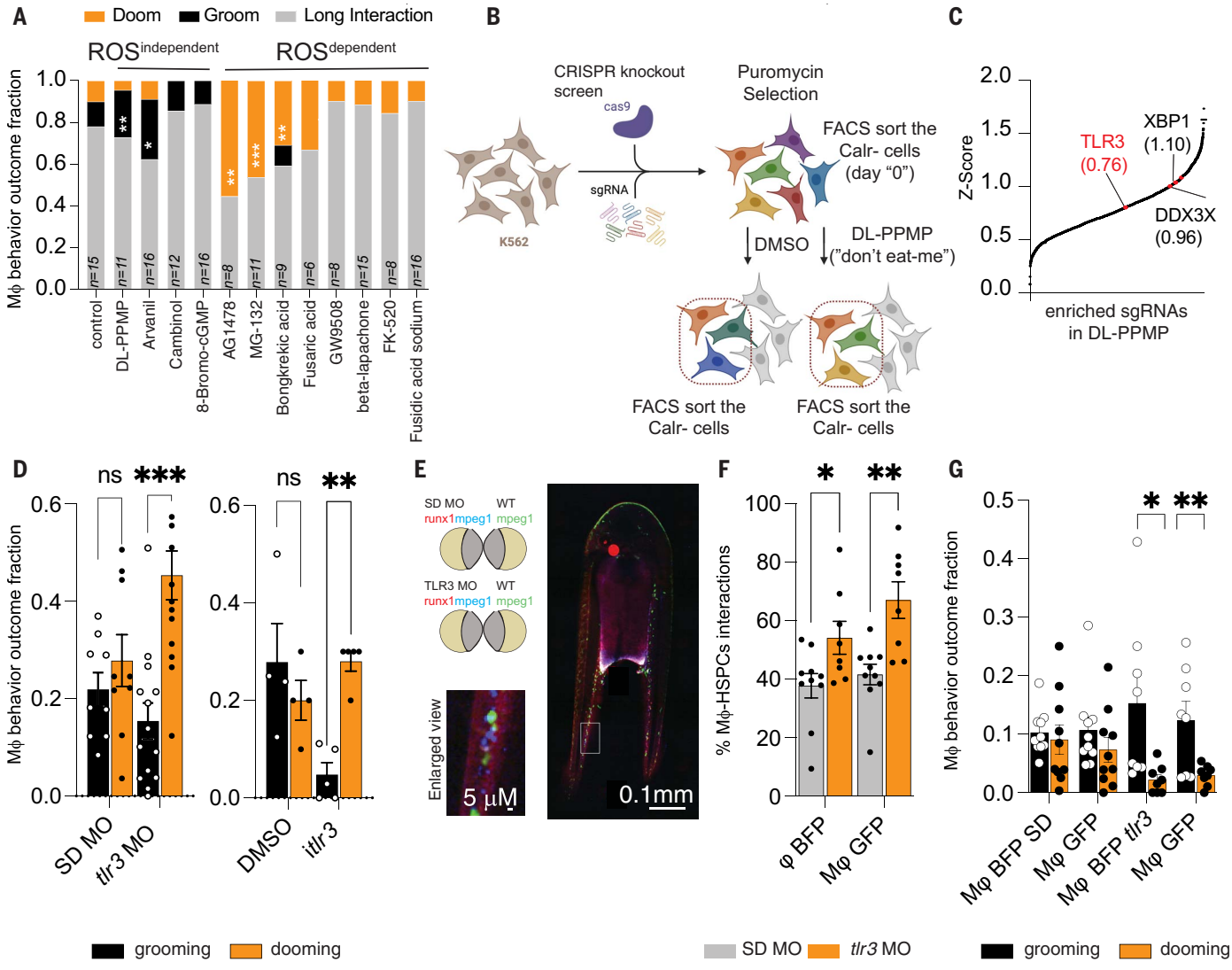

Fig. 2. Tlr3 is required for HSPC grooming. (**A**) Stack Plot showing the macrophage interaction behavior in the presence of the Calr inducers. Grooming behavior is shown in the black bar, and dooming behavior as the orange bar. The imaging was conducted using 3-dpf zebrafish embryos. The exact sample size is indicated in the figure. *n* = 6 to 16 from two independent experiments. Data were analyzed by Wilcoxon matched-pairs signed rank test. **P* = 0.0156, ***P* = 0.002, ****P* = 0.001. (**B**) Schematic overview of the Gecko 2.0 CRISPR-Cas9 knockout screen. (**C**) sgRNAs significantly enriched (*P* < 0.05) were identified using MAGECK software and plotted as a cumulative stack on the basis of their *Z* score. The arrows indicate examples of significantly enriched sgRNAs, and their *Z* score is depicted inside the brackets. The screen was conducted using K562 cells. The screen was performed in three independent experiments. (**D**) Knock-down of *Tlr3* (Tlr3 MO) or iTlr3 treatment reduces the fraction of HSPCs that are groomed but increases the fraction of HSPCs that are doomed in 3-dpf zebrafish embryos. The macrophage behavior outcome fraction was calculated by counting the total number of interacting macrophages and dividing by the total number of dooming or grooming events. Data points represent an image embryo: SD MO, *n* = 9; *tlr3* MO, *n* = 11; DMSO, *n* = 4; and iTLR3, *n* = 5. Two independent experiments were performed. Two-way ANOVA followed by Sidak's multiple comparisons test was used. ***P* = 0.0027; ****P* = 0.00005. (**E**) Representative imaging showing the experimental design of the parabiosis experiment. (**F**) Both macrophages showed higher interaction rates with the HSPCs. **P* = 0.04, ***P* = 0.0015. Data were analyzed using a two-way ANOVA test. The macrophage-HSPC interaction percentage was calculated by counting the total number of HSPCs (runx1$^+$ cells) and dividing by the total number of HSPCs interacting with a macrophage. (**G**) Bar plot showing the macrophage behavior outcome fraction. The macrophage behavior percentage outcome was calculated by counting the total number of interacting macrophages and dividing by the total number of dooming or grooming events. **P* = 0.01, ***P* = 0.0057. Data were analyzed using an unpaired Student's *t* test. For (F) and (G), data points represent an image embryo. *n* = 10 from three independent experiments.

Despite a reduction in Calr$^+$ HSPCs, *tlr3* depletion by morpholino or iTlr3 increased dooming and decreased grooming (Fig. 2D and movies S3 to S5). To address potential cell-autonomous defects in macrophage behavior, we performed parabiosis experiments in which standard or *tlr3* morpholino–injected embryos from the *runx1*$^+$*23mCherry*;*mpeg1*:BFP were fused to a *mpeg.1:EGFP* WT zebrafish (Fig. 2E). Macrophages of both origins, WT (green) and *tlr3* morphants (blue), showed the same increased engagement to HSPCs, followed by increased dooming behavior. This demonstrated that Tlr3 acts in a HSPC-autonomous manner to prevent dooming behavior (Fig. 2, F and G). To investigate whether Tlr3 was sufficient to promote grooming, we sorted murine lineage$^-$Sca1$^+$cKit$^+$ (LSK$^+$) HPSCs, pretreated them with either poly I:C, a dsRNA mimic (Tlr3 agonist) (*19*), or DMSO, and cocultured them with their autologous bone marrow–derived

macrophages (BMDMs). We observed that poly I:C-pretreated HSPCs showed higher grooming ratios (fig. S2, J and K), ergo suggesting that Tlr3/dsRNA signaling in HSPC promoted grooming behavior.

Tlr3 signaling directs HSPC surface presentation of B2m

To gain insight into the molecular mechanism triggered by the "don't eat-me" compound DL-PPMP, we analyzed previously available bulk RNA-sequencing (RNA-seq) data from a DL-PPMP–treated human cancer cell line (*20*). We identified 2285 up-regulated genes in treated cells that were enriched for pathways associated with the viral immune response, such as regulation of interferon-α (IFN-α) production, antigen processing, and presentation of endogenous peptides through MHC class I. Consistent with our data, K562 cells treated with DL-PPMP expressed higher levels of B2m, a molecule required for the MHC-I stabilization on the cell surface (fig. S3A). Although MHC-I is required for antigen presentation and $CD8^+$ T cell activation (*21*), it can also prompt a "don't eat-me" signal (*22*). For example, MHC-I–B2m expression protects cancer cells from phagocytosis through engagement of LILRB1/LILRB2 expressed in immunosuppression-related cells, such as tolerogenic dendritic cells and M2-type macrophages (*22*–*24*).

Evolutionarily, this mechanism might be conserved because, based on data from Actinopterygii, the LILR system originated 450 million years ago, and the leukocyte immune-type receptor (LITR) shows orthologous relationship to the human LILR receptor (*25*, *26*). On the basis of our CRISPR-screen to identify the molecular cues of surface Calr inducers in the "don't eat-me" context (Fig. 2C) and results showing that Tlr3 facilitated grooming (fig. S2, J and K), we hypothesized that HSPCs would display more B2m in response to Tlr3 signaling, thereby suppressing macrophage phagocytosis and preventing dooming behavior. To test this hypothesis, we evaluated surface levels of B2m on HSPCs in *tlr3* zebrafish morphants. We found that depleting *tlr3* in zebrafish embryos resulted in fewer $B2m^+$ HSPCs (fig. S3B). Considering that *tlr3* zebrafish morphants showed higher dooming events (Fig. 2D), our results suggested that the lower B2m expression resulting from lower Tlr3 expression biased the HSPCs to be doomed by the macrophages.

Surface B2m determines the outcome of macrophage-HSPC interactions mediated by Calr

We treated 48 hpf zebrafish embryos with ROS-independent compounds and evaluated the surface B2m on HSPCs using fluorescence-activated cell sorting (FACS). We found that ROS-independent compounds increased B2m levels (fig. S3, C and D, blue), whereas "eat-me" or iTlr3 treatments decreased surface B2m levels (fig. S3, C and D). To validate whether the signal input provided by Calr and B2m was important for the outcome of macrophage-HSPC interactions, we used CRISPR-Cas9 to generate zebrafish crispant embryos with mosaic deletions of *b2m* and treated them with ROS-independent Calr inducers. DMSO was used as the vehicle control in the embryos injected with control sgRNA and *b2m* sgRNA. Upon *b2m* depletion, ROS-independent Calr inducers promoted dooming rather than grooming (fig. S3E). Together, these data support the hypothesis that ROS-independent Calr inducers promote grooming through both Calr and B2m surface presentation, with Calr promoting the macrophage-HSPC interaction and B2m providing the "don't eat-me" signal hindering HSPCs from being fully engulfed by macrophages.

Mosaic crispants are limited by editing efficiency. Thus, to confirm the role of B2m in macrophage-mediated HSPC grooming, we generated *b2m*-stable knockout zebrafish. We used CRISPR-Cas9 to cause a frameshift mutation in the 3-exon of the *b2m* gene in zebrafish with a *runx1*$^+$*23:mCherry;mpeg1-EGFP* background. We investigated the outcome of macrophage-HSPC interactions in these homozygous mutants by live-cell imaging at 72 hpf. *B2m* depletion promoted HSPC dooming and decreased HSPC grooming (Fig. 3, A to E, and fig. S3D), which further supports the role of surface B2m as a "don't eat-me" signal on HSPCs. This increase in dooming was not associated with increased numbers of $Calr^+$ HSPCs (fig. S3G). Also, despite the low surface Calr on HSPC surfaces, we observed fewer $Runx1^+$ cells in the caudal hematopoietic tissue (CHT) (fig. S3H), potentially indicating enhanced HSPC dooming.

Next, to validate the role of B2m as a "don't eat-me" signal, we treated our *b2m*-knockout embryos with the ROS-independent compound DL-PPMP. We rationalized that DL-PPMP would increase surface Calr (increasing macrophage-HSPC interactions), but that in the absence of B2m, the interactions would lead to dooming. We observed that DL-PPMP stimulated interactions in both WT and *b2m*-knockout embryos. However, *b2m*-knockout HSPCs were doomed, whereas WT HSPCs were groomed (Fig. 3, F and G). These results supported the importance of surface B2m to instruct grooming behavior by the macrophages.

We then sought to evaluate whether the "don't eat-me" signal mediated by B2m was conserved throughout evolution. To this end, we sorted murine HSPCs (LSK^+) that were $MHC\text{-}I^+$ or $MHC\text{-}I^-$ and co-cultured them with BMDMs for 4 hours (Fig. 3H). We opted to sort for MHC-I because its surface expression is dependent on the presence of B2M. We found that murine $MHC\text{-}I^+$ HSPCs promoted macrophage grooming (Fig. 3I). Overall, these results showed that B2m decorates the surface of HSPCs and promotes the "don't eat-me" signal during the macrophage-HSPC interactions.

B2m is required for safeguarding HSC clonal complexity

As in *B2M* germline mutations in mammals (*27*), we did not observe major changes in development after *b2m* knockout in adult zebrafish, except for a decrease in lymphoid cells (fig. S3I) that possibly reflected impaired $CD8^+$ differentiation (*28*).

HSC clonal complexity is essential for maintaining a functional and resilient immune system, supporting long-term hematopoietic function, and reducing the risk of hematological diseases (*29*, *30*). Because grooming and dooming regulate HSC clonal complexity (*6*), we sought to determine whether B2m depletion could affect the HSC clonal landscape. We hypothesized that increased dooming in *b2m* mutants reduces the number of HSC clones in adulthood. To test this, we generated mosaic deletions using tissue editing with inducible stem cell tagging through recombination (TWISTR) to combine CRISPR-Cas9–mediated gene editing with Zebrabow (zbow) HSC color labeling (*31*, *32*), which allows mutant and WT stem cells to compete in vivo. *Zebrabow-M;draculin:CreERT2* embryos permit specific lineage labeling of individual HSC clones at 24 hpf (Fig. 3J). Mosaic deletion of *b2m* reduced the number of myeloid and lymphoid or progenitor clones (fig. S3J) and promoted clonal dominance (Fig. 3, K to M, and fig. S3K). Additionally, macrophage ablation before HSPC lodgment in CHT rescued clonal dominance in *b2m* crispants (Fig. 3, K to M) but did not rescue clone numbers (Fig. 3M). The decrease in clone numbers may reflect the impairment of Il-1β–driven proliferation (*6*), therefore limiting the number of HSC clones (Fig. 3N). Considering the mosaic nature of TWISTR, we hypothesized that the more abundant (or dominant) clones found in the *b2m* mutation condition are WT cells that do not carry *b2m* mutation. Therefore, we sorted dominant and nondominant clones and evaluated their *b2m*-editing efficiency. Indeed, dominant clones were WT for *b2m*, suggesting that *b2m* mutant clones were doomed and led dooming-resistant WT clones to overtake the adult marrow (fig. S3K). These results indicate that B2m decorates the surface of HSPCs and protects them against macrophage removal, thus affecting HSPC clonality in adulthood.

Interferon-regulatory factor 3 (Irf3) mediates a Tlr3/Tlr4–specific antivirus gene program upstream of *b2m* expression (*33*–*35*). We therefore used the TWISTR system to generate TWISTR-*irf3* mutants to elucidate the molecular pathways that regulate HSC clonality through B2m. We also generated TWISTR-*tlr3* mutants and treated zebrafish embryos with iTlr3

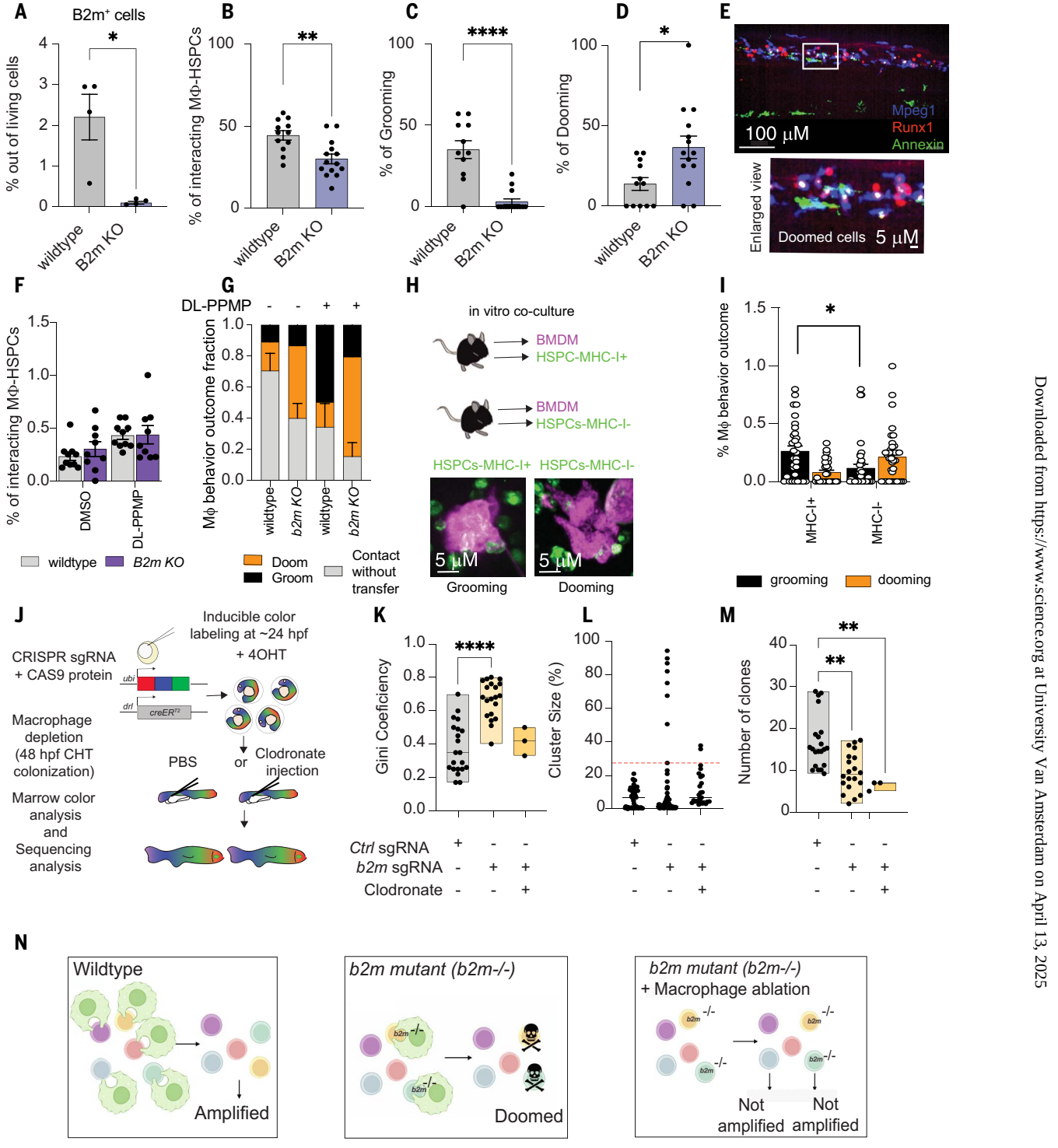

Fig. 3. B2m acts as a "don't eat-me" molecule and prevails unwarranted HSPC dooming. (**A**) *b2m* knock-out stable mutants (*B2m KO*) showed a significant reduction in B2M levels. Data were analyzed by unpaired Mann-Whitney *U* test. **P* = 0.028. Data points represent a pool of 100 embryos. (**B**) Barplot showing the interaction percentage. (**C** and **D**) *b2m* KO embryos showed significantly lower macrophage-HSPC interaction with a dooming dominance. Data were analyzed by unpaired Mann-Whitney test. **P* = 0.012, ***P* = 0.0021, *****P* < 0.0001. Data points represent an image embryo. WT, *n* = 12; B2m KO, *n* = 14. Data represent three independent experiments. The macrophage-HSPC interaction percentage was calculated by counting the total number of HSPCs (runx1$^+$ cells) and dividing by the total number of HSPCs interacting with a macrophage. (**E**) Representative imaging showing the increased dooming behavior observed in the *B2m*-homozygous mutant. *n* = 4 from two independent experiments. (**F**) Bar plot showing the interaction rates in WT and *B2m* KO zebrafish embryos. *n* = 4. Data points depict the field of view. (**G**) The macrophage behavior percentage outcome was calculated by counting the total number of interacting macrophages and dividing by the total number of dooming or grooming events. Whereas in the WT background DL-PPMP promoted grooming, in the *B2m* KO background, it promoted dooming. (**H**) Schematic overview of the murine HSPCs (LSK$^+$) and macrophage

co-culture. Left bottom panel is a representative imaging showing the sorted murine HSPC-MHC-I$^+$ (green) being groomed by a macrophage (magenta). Right bottom panel is a murine HSPC-MHC-I$^-$ being doomed by a macrophage. (**I**) MHC-I$^+$ HSPCs showed higher grooming rates compared with MHC-I$^-$ cells. Data were analyzed using nonparametric one-way ANOVA followed by Kruskall Wallis test. *P = 0.03. Data are shown as means ± SEM. The macrophage behavior outcome fraction was calculated by counting the total number of interacting macrophages and dividing by the total number of dooming or grooming events. (**J**) Schematic overview of the *Zebrabow-M* system. Animals with 15 to 20 insertions of a multicolor fluorescent cassette were crossed to the *draculin:CreERT2* line to enable clonal labeling of lateral plate mesoderm lineages. By treating with 4-OHT at 24 hpf, just after HSC specification, individual stem cell lineages expressing specific fluorescent hues can be quantified in the adult marrow. (**K**) Families of *Zebrabow-M;draculin:CreERT2* animals injected with *b2m* morpholino with or without clodronate liposomes exhibited reduced numbers of HSC clones. (**L** and **M**) Clonal dominance in the adult marrow. Clodronate liposome was injected at 48 hpf. Data points represent an adult kidney marrow. Control, n = 22; b2m sgRNA, n = 21; and clodronate, n = 3. Experiments were conducted at least twice. For (A) to (D), (F), (G), and (I), and (K) to (M), data are shown as means ± SEM. Experiments were conducted in vivo using zebrafish as a model. (**N**) Schematic overview of the clonal diversity in regard to the "don't eat-me" signal.

to suppress Tlr3 and dsRNA downstream signaling at 48 hpf. Like *b2m* mutants, mosaic depletion of *irf3* and *tlr3*, as well as inhibition of Tlr3 signaling, reduced the number of myeloid clones while increasing clonal dominance (fig. S3, L to Q). The TWISTR-*irf3* mutants similarly showed WT clonal dominance, indicating a competitive disadvantage of *irf3*-depleted stem cells (fig. S3, L to N). Alongside the imaging results, this shows that both B2m mutant HSCs and Irf3 mutant HSCs are removed by macrophages because the cells no longer present the "don't eat-me" signal. These data suggest an operative molecular network of Tlr3 activation cascades that promote Irf3 activation (*36*), which could promote the transcription of *b2m*.

Cytosolic dsRNAs promote B2m expression and protection from dooming

Increased expression of *b2m* is a classic response against viral infection and a cellular response to type I IFN (*37*–*39*). To investigate the intrinsic heterogeneity of the HSPC population, we used the IFN-stimulated gene 15 (*isg15*) as a reporter for the Tlr3-mediated Irf3 response (*37*–*39*). Flow cytometry revealed that 27% of Runx1$^+$ HSPCs were positive for *isg15* (Fig. 4A and fig. S4A) and positively correlated with B2m surface presentation (Fig. 4B). Isg15$^+$ HSPCs were less likely to be doomed by macrophages (Fig. 4C and movie S6). The associated enrichment of *isg15* activity and B2m within select HSPCs hinted at a viral mimicry response in these cells. To test this, we injected 72-hpf embryos with a Tlr3 agonist, poly I:C, and measured the fraction of Isg15$^+$ HSPCs. We found that poly I:C increased the fraction of Isg15$^+$ HSPCs (fig. S4B). Collectively, these data suggest an endogenous, viral mimetic response could trigger the type I IFN pathway, leading to high B2m levels on the HSPC surface and consequently protect the HSPCs from dooming.

REs, including endogenous retrovirus (*Erv*), have roles in regulating HSPC formation and regeneration. Therefore, we hypothesized that REs could be the endogenous Tlr3 ligand mediating *b2m* expression (*40*–*42*). Quantitative polymerase chain reaction (qPCR) analysis of Runx1$^+$Isg15$^+$ cells revealed a consistent increase in endogenous retroviral and B2m expression (Fig. 4D). These data suggested that HSPCs with higher levels of RE transcripts also have elevated levels of B2m.

To gain insight into the RE status in macrophage-interacting HSPCs, we reanalyzed published single-cell RNA-seq data of sorted *runx1*$^+$*23:mCherry* HSPCs from macrophage-depleted and control embryos (*6*) and modified the mapping to include the expression of REs, including long terminal repeats (LTRs), at the single-cell level (*43*). The cluster of cells enriched for cell cycle gene expression (cluster 2) had elevated RE expression compared with the cluster enriched for noncycling cells (Fig. 4, E and F, and fig. S4C). This suggested that HSPCs that are primed to proliferate have higher RE expression. Additionally, bulk RNA-seq of Runx1$^+$ cells from the CHT of embryos treated with DL-PPMP, a pro-grooming, B2m-dependent compound, showed an up-regulation of REs, including transcripts for *ltrs* (fig. S4D).

To evaluate B2m expression in HSPCs carrying high or low content of *Erv* transcripts, we crossed a zebrafish reporter line for a zfERV (LTR5) (*44*) with *runx1*$^+$*23:mCherry* zebrafish. LTR5$^+$ HSPCs exhibited higher B2m levels by FACS (fig. S4E). We next sought to determine whether RE levels were dependent on macrophage-HSPC interactions. To test this, we quantified the levels of cytosolic dsRNA in Runx1$^+$ cells from WT or macrophage-depleted embryos at 48 hpf. Macrophage depletion did not change the dsRNA content in Runx1$^+$ cells (fig. S4F), suggesting that the endogenous content of REs in HSPCs is independent of macrophage interaction.

Overall, these data demonstrated that elevated cytosolic REs, including *LTRs*, correlated with higher B2m levels, suggesting that a viral mimicry program could protect HSPCs from macrophage dooming.

To determine whether inducing the expression of RE in HSCs could regulate macrophage behavior, we treated 48-hpf zebrafish embryos with the G9a/DNMT inhibitor CM272 (*45*). We reasoned that inhibiting DNA methylation would enhance RE expression, including *Erv* (*46*, *47*). Indeed, after 24 hours, HSPCs from embryos treated with CM272 showed increased expression of endogenous retrovirus and virus-like response genes (fig. S4G). Additionally, CM272 increased the proportion of Isg15$^+$ and B2m$^+$ HSPCs and increased the level of Calr on HSPCs (fig. S4, H to K). This suggested that CM272 could promote HPSC grooming by macrophages. We treated 72-hpf embryos with CM272, which increased HSPC proliferation and the number of Isg15 HSPCs and reduced HSPC dooming in live imaging experiments (Fig. 4, G to I, and movies S7 and S8).

Because CM272 might have the potential to regulate dooming and grooming through a number of gene expression changes beyond up-regulation of REs, we cloned the zebrafish *ltr4* downstream of the *runx1*$^+$*23* enhancer GFP to promote the overexpression of a RE in the HSPCs. We found that HSPCs from embryos overexpressing *ltr4* (*ltr4-OE*) showed higher proliferation compared with embryos overexpressing the *runx1*$^+$23 enhancer GFP (fig. S4L). Considering that macrophage grooming and longer interactions correlate with higher HSPC proliferation (*6*), the increased proliferation observed in the *ltr4-OE* may reflect higher grooming behavior. Thus, increasing global RE expression (by CM272) or overexpression of a specific RE (Ltr4) protected against macrophage dooming.

We investigated the potential consequences of RE-mediated protection from reduced dooming events on HSPC clonality. We opted to use CM272 treatment as a tool to increase the "don't eat-me" signal on HSPCs because it enabled us to focus on the events after HSPC budding (which occurs at 24 to 48 hpf). We reasoned that the derepression of retroviral elements would increase the proliferation of HSPCs. Indeed, CHT imaging confirmed higher proliferation rates of HSPCs, as depicted by 5-ethynyl-2′-deoxyuridine (EdU) incorporation (Fig. 4H). However, zebrabow analysis showed virtually no difference in clonality (Fig. 4, J and K), suggesting that CM272 promotes the amplification of already established clones. We did not observe a rescue in clonal dominance when we treated TWISTR-*b2m* mutants with CM272, confirming that dsRNA sensing occurs upstream of B2m presentation. (Fig. 4, J and K).

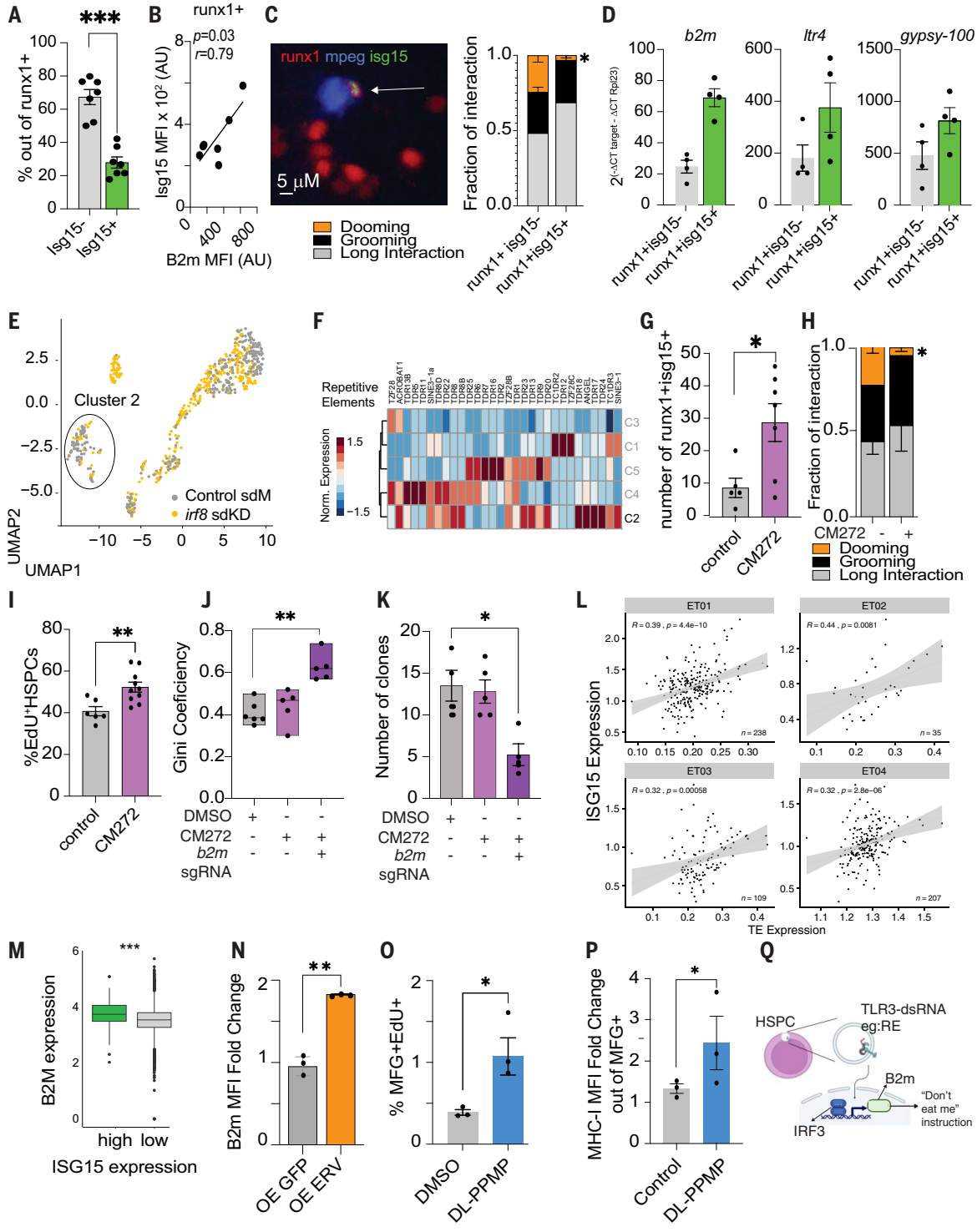

Fig. 4. REs as *Erv* elicit a virus-like response in HSPCs promoting B2m expression. (**A**) Flow cytometry showing that ~20% of *runx1*$^{+}$*23mCherry*$^{+}$ HSPCs express Isg15 (gating strategy is shown in fig. S4A). Data points represent a pool of ~200 embryos acquired in three independent experiments. Data are shown as means ± SEM. Data were analyzed with Mann-Whitney test. *P* = 0.003. (**B**) Positive correlation between B2m and Isg15 levels. Data were analyzed by Pearson correlation. Data points represent a pool of ~200 embryos acquired in three independent experiments. (**C**) Left: representative image of a Isg15^{+}-HSPC interaction. HSPCs are shown in red, macrophages in blue, and isg15 in green. Right: HSPCs-Isg15^{+} cells showing lower dooming ratios. (**D**) Sorted *isg15*$^{+}$ HSPCs showing higher *b2m* and RE expression. Data points represent a pool of ~200 embryos. Experiments were performed twice. The *y* axis depicts the relative gene expression. (**E**) Uniform manifold and projection (UMAP) of sorted *runx1*$^{+}$*23-mcherry* HSPCs in standard morpholino (gray, control sdM) and *irf8*-depleted embryos (yellow, *irf8* sdKD). [Original data are from Wattrus *et al.* (*6*)]. (**F**) Cluster 2 (C2), enriched for control HSPCs, showing higher expression of RE. A total of 808 cells were analyzed. (**G**) Treating 2-dpf embryos with CM272 (5 uM) led to higher number of isg15^{+}HSPCs in the 3-dpf CHT. Data were quantified by live-cell imaging and analyzed by Mann-Whitney test. **P* = 0.02. Data points represent an embryo. Experiments were performed

twice. (**H**) EdU staining of *runx1*$^{+}$*23:mCherry* embryos treated with CM272 identifies a significant increase in proliferating HSPCs at 3 dpf. Data were analyzed by Student's *t* test. Data normality was enquired by the Shapiro-Wilk test. $^{**}P$ = 0.0061. Data are shown as means ± SEM. Control, *n* = 5; CM272, *n* = 7. (**I**) CM272-treated embryos showed lower dooming ratios. Data points represent an embryo. Percentage was calculated by quantification of Edu^{+} Runx1^{+} cells divided by the total number of runx1^{+} cells. The plot depicts two independent experiments. Control, *n* = 6; CM272, *n* = 10. (**J**) Gini coefficient in control (DMSO), CM272, and CM272 *b2m*-knockdown zebrafish. Data were analyzed by Kruskall-Wallis test followed by Dunn's multiple-comparisons test. $^{**}P$ = 0.0043. Data points represent an adult fish. DMSO, *n* = 6; CM272, *n* = 5; and b2m sgRNA, *n* = 5. The plot depicts two independent experiments. (**K**) *b2m*-TWISTR *Zebrabow-M;draculin:CreERT2* treated CM272 exhibits reduced numbers of HSC clones in the adult marrow. Data were analyzed by Kruskall-Wallis test followed by Dunn's multiple-comparisons test. $^{*}P$ = 0.023. Data points represent an adult fish. DMSO, *n* = 6; CM272, *n* = 5; and b2m sgRNA, *n* = 5. The plot shows two independent experiments. (**L**) *ISG15* expression positively correlates with transposable element (TE) expression in human HSCs. Previously published single-cell RNA-seq datasets of human bone marrow CD34^{+} stem and progenitors [original data from Nam *et al.* (*90*), *n* = 4 samples] were aligned to a TE reference using CellRanger v3.2. TE expression was normalized by total RNA counts. Pearson correlation was performed between TE expression and *ISG15* gene expression of individual HSCs, represented in each data point. (**M**) Human bone marrow HSCs from the same dataset as in (L) were grouped based on their *ISG15* expression, where in the upper quartile was considered the threshold for high and the lower quartile as low. Normalized expression of *B2M* is shown for individual cells. *ISG15* high cells showed higher *B2M* expression. Only cells with at least one transcript of *ISG15* were included in the analysis. High, *n* = 203 cells; low, *n* = 608 cells from *n* = 4 samples. *P* = 0.02 using a linear mixed model, with sample as a random effects variable. Box plot represents the median; in the bottom and top quartiles, whiskers correspond to 1.5× the interquartile range. (**N**) Human *Erv* overexpression was up-regulated the B2M levels on human CD34^{+} cells. Data are shown as means ± SEM. Data points depict a CD34 donor. Data were collected from two independent donors. (**O**) EdU staining of MFG^{+} mice treated with DL-PPMP identifies an increase in proliferating HSPCs 24 hours after the treatment. Percentage was determined by the total number of living cells. Data points depict a mouse. (**P**) DL-PPMP treatment stimulates B2M expression in murine HSPCs. Flow cytometry was performed using the cells from the tibia and femur (for gating, see fig. S4Q). Data were analyzed by Student's *t* test. $^{*}P$ = 0.02. Data are shown as means ± SEM. *n* = 3 mice per condition. (**Q**) Schematic overview of the proposed molecular pathway resulting in higher surface B2m.

These data showed that REs positively correlated with B2m^{+} HSPCs and that upregulating endogenous retroviral levels could provide protection against HSPC dooming.

B2m induction through endogenous retrovirus is conserved throughout evolution

The sequence of amino acids for B2m is highly conserved (*48*, *49*). Therefore, we investigated whether ERV-driven B2M expression is conserved in mammals. Consistent with our observation in zebrafish, we found that human *ISG15*$^{+}$ HSPCs (*50*) had higher *B2M* expression and were positively correlated with the expression of REs (Fig. 4, L and M).

We overexpressed human *Erv* or *GFP* (as a control) in CD34 cells to validate a causal relationship between B2M levels and RE expression. Overexpression of *ERV*, but not control GFP, led to an increase in B2M on the surface of HSPCs (Fig. 4N and fig. S4, M and N). By contrast, ROS levels were not elevated after *ERV* overexpression (fig. S4M). The surface B2m increase was observed in CM272- and poly I:C–treated human CD34 cells, and this could be abrogated by blocking TLR3 signaling (fig. S4O). Our data from human cells and zebrafish suggested that the regulation of B2M through dsRNA/TLR3 signaling is conserved throughout evolution.

To understand the functional relevance of the "don't eat-me" signal in the mammalian system, we treated myelodysplastic syndrome 1 (*Mds1*)$^{GFP+}$/*Flt3*^{Cre} (MFG) stem cell reporter mice (*51*) with DL-PPMP because it promotes the presentation of B2M, but not other "don't eat-me" molecules such as CD47 (fig. S4P). We chose this reporter model because *Mds1* is a gene highly enriched in long-term HSCs that are capable of self-renewing (*52*). We found that DL-PPMP treatment increased HSPC proliferation (Fig. 4O and fig. S4Q) and increased MHC-I levels (Fig. 4P and fig. S4Q), suggesting that the HSPCs were protected from macrophage dooming and proliferated as a consequence of grooming.

B2m expression in response to REs alters HSPC fate

Endogenous retroviral proteins and genetic material have already been shown to regulate the innate immune response (*53*, *54*). ERV-derived enhancers and promoters appear to be activated upon pathogen infection, suggesting a cooperative activation in responding to pathogens (*55*, *56*) or the existence of a trained immunity (*57*) function between the innate immune response and ERVs.

Given the evolutionary conservation of RE and B2M, we then sought to investigate the relevance of this finding in the context of pathogen infection, which is an evolutionarily conserved process. We evaluated the role of Tlr3 signaling in mediating "emergency granulopoiesis." This is a distinctive, protective program of accelerated de novo production of neutrophils from amplification of progenitor cells in response to fatal infection (*58*, *59*). Therefore, to determine whether poly I:C could induce emergency granulopoiesis, we treated zebrafish embryos with poly I:C and assessed the numbers of neutrophils as a proxy for a myeloid emergency response. We found that upon poly I:C stimulation, the population of neutrophils increased (fig. S4R). Similarly, humanized NOG mice showed higher granulopoiesis and granulocyte-macrophage colony-stimulating factor levels upon infection (*60*). Although further studies are needed to strengthen the relevance of this phenomenon, our results suggest that viral stimulation may confer a better fit against opportunistic pathogens by promoting granulocyte differentiation.

In addition to the pathogenic aspects, we also found higher *B2M* expression in acute myeloid leukemia (AML)–malignant HSPCs and higher TE expression in human AML blast cells (fig. S5, A and B). This suggested that AML cells might hijack the "don't eat-me" signal to avoid macrophage elimination.

Our data demonstrate that viral-mimetic signaling of RE-Tlr3 mediates surface-level B2m on HSPCs to promote macrophage-mediated grooming and protect against macrophage dooming in an evolutionary conserved manner that shapes HSC fate determination and clonal proliferation (Fig. 4Q).

Discussion

Our data support a model in which macrophages vet the quality of newly formed HSPCs through a balance between "eat-me" and "don't eat-me" signals. This process is mediated by the inputs provided by surface Calr ("eat-me") and B2m ("don't eat-me"), which are driven by ROS and dsRNA-Tlr3 signaling, respectively. In our proposed model, surface Calr governs the macrophage-HSPC interaction, and B2m, a "don't eat me" signal, dictates macrophage grooming or dooming behavior.

B2m is an evolutionarily conserved molecule that positively responds to type I IFN (*49*, *61*–*65*). The IFN family has been previously reported to break stem cell quiescence to promote asymmetric division (*66*, *67*) and stimulate embryonic HSC maturation (*68*). Type I IFN regulates the Jak-Stat pathway, mediated by STAT1 phosphorylation, resulting in HSC proliferation and activation. Our work expands the implications of type I IFN because it shows that a Tlr3/dsRNA cascade triggers an Irf3 response that stimulates the expression of B2m on HSPCs. B2m acts as a "don't eat-me" signal, thereby inhibiting macrophage dooming

of HSPCs. We envision that our findings on the influence of B2m extend beyond the hematopoietic system, affecting tumor-associated macrophages (*22*, *69*–*71*) and anti-CD47 treatment efficacy in tumors with high MHC-I (*22*). In species such as zebrafish that lack CD47 orthologs, our work suggests B2m as a primitive signal on stem cells for mediating the "don't eat-me" signal in macrophages.

We uncovered the role of RNA REs in regulating stem cell clonality by triggering Tlr3, mimicking a virus response that will result in the expression of B2m, a "don't eat-me" molecule. Other TLR responses may mediate Calr externalization. For example, viruses such as flaviviruses (single-stranded RNA, TLR7/8) can promote the externalization of Calr, which in turn is recognized by natural killer (NK) cells (*72*). B2m, which curtails macrophage-mediated engulfment, could also attenuate NK cell activity. ERV activation may accelerate the differentiation of HSPCs to immune cells, which would help fight infection, thus providing an evolutionary selection to maintain HSPCs that have endogenous ERV activation. Our experiments using the demethylating agent CM272 demonstrate that derepression of RE triggers B2m, and this is associated with clonal persistence. Patients with myelodysplasia and leukemia are often successfully treated with demethylating agents (*73*–*76*), and it is possible that the therapeutic response is caused by RE activation and the survival of normal or mutant clones associated with adequate differentiation by the "don't eat-me" signal.

In the development context, REs have been shown to increase expression of RE RNA during the endothelial-to-hematopoietic (ETH) transition, during which they mediate HSPC formation (*40*). isg15^{+} HSPCs could be responding to REs in a manner reminiscent of the ETH process. In this scenario, the RE-harboring HSPCs from ETH would respond to the IFN program, enabling the expression of B2m and competition for marrow colonization. This protective mechanism may also operate in adulthood in response to environmental stress, such as during infections or in clonal stem cell disorders such as leukemia. Supporting this hypothesis, transposable element expression were used to accurately predict AML prognosis (*77*). B2m could confer protection of myelodysplastic or leukemic clones, resulting in the establishment of the diseases. Manipulating the levels of "don't eat-me" and "eat-me" signals may thus have important therapeutic implications for immune therapy by harnessing the macrophage-selective removal of a mutated stem cell clone.

Materials and methods

Animal models

WT zebrafish AB, *casper* or *casper*-EKK (*78*), and transgenic lines, *runx1*$^{+}$*23:mCherry* (*11*), *Zebrabow-M draculin:CreER*^{T2} (*31*, *79*), *mpeg1:BFP* (*6*), *mpeg1:EGFP* (*80*), *ltr5-EGFP* (*44*), *isg15-EGFP* (*39*), *Calr3a knockout* (*from ZIRC*), and *irf8 knockout* were used. For the embryonic experiments, we used 3-dpf embryos, whereas the adult experiments were conducted in 4- to 6-month-old fish. Both genders were used for the experiments.

WT 8- to 12-week-old male and female C57BL/6J mice (Jackson Laboratories, stock no. 000664) were also used in this study. All mice were housed in the animal facility of Harvard University or at the Boston Childrens Hopital mouse house, and all experiments and protocols were performed in compliance with the institutional guidelines of Harvard University. The animals were kept under ad libitum food and water and euthanized by CO_2 asphyxiation

All animals were housed at the Faculty of Art and Science of Harvard University and handled and all procedures were approved by the institutional animal care and use committee of Harvard University protocols (15-03-237 and 11-21-3).

Chemical screen

HEK293 cells transfected with the SPLIT-Turbo ID (*9*) constructs were treated with the Sigma Lopac 1280 chemical library and BIOMOL/ICCB bioactive. Chemical libraries were in a 384-well format and were diluted into the 384-well format using robots. The final chemical compound concentration was 5, 2.5, and 0.625 μM in a final treatment volume of 50 μl of RPMI supplemented with 10% fetal bovine serum (FBS), 1% glutamine, 1% pen/strep, and 100 μM biotin. After 24 hours, the cells were manually stained with streptavidin (catalog no. 405235, BioLegend), A647-zenon (Thermo Fisher, Z-25408) conjugated Calr (Thermo Fisher, catalog no. PA3-900), and Hoechst (Invitrogen, catalog no. H3570). Screening of inducers and in vivo was performed using a Zeiss Cell Discoverer 7 Live/High content equipped with the Prime 95B camera with control CO_2 and temperature. Cell profiler objected to identification, and the R package "R sight" was used to identify the chemical hits inducing surface Calr. The wells treated with DMSO were used as a control.

Genome-scale CRISPR-Cas9 knockout screening in human cells

The human GeCKO v2 one-plasmid system library was purchased from Addgene (catalog no. 52962) (*13*, *81*). This one-plasmid system contains a lenti/Cas9-blast plasmid. The amplification of these plasmids and lentiviral production was performed following the protocol described by Shalem *et al.* (*13*)

K562 cells were cultured until 80% confluence and transduced using spintransfection, and then 100 × 10^6 cells were transferred to a 1.5-ml microtube containing 8 mg/ml polybrene (Millipore, catalog no. TR-1003-G) and the lentiviral library. The multiplicity of infection (MOI) used CRISPR library transduction was of 0.3 to limit multiple lentiviral integration. Then, samples were centrifuged at 1000*g* for 2 hours at 34°C. After infection, the cells were resuspended in Iscove's modified Dulbecco's medium (IMDM) (catalog no. S11150H) with 10% FBS (catalog no. F22100) and 1% glutamine to remove the remaining polybrene and nontransfected virus. After 24 hours of recovery, puromycin (1 μg/ml) was added to the culture to select the cells carrying the constructs. The cells were kept for 5 days under these conditions.

After puromycin selection, the cells were centrifuged at 500*g* for 5 min and resuspended in 10% IMDM supplemented with DMSO (vehicle control) or DL-PPMP (5 μM). The cells were stimulated for 24 hours; 10^6 were kept for baseline correction (day 0) and labeled with zenon-conjugated Calr (A647). The Calr^{-} cells were sorted in a FACSAria cell sorter (BD Biosciences). Before FACS sorting, cells were treated with Zombie Dye (BioLegend) for cell viability.

Gecko library preparation

At the end of the screen, the library preparation was generated by deep sequencing of nested PCR amplicons (*82*). In brief, genomic DNA from Calr^{-} sorted cells was extracted with DNeasy blood and tissue kit (Qiagen, catalog no. 69506). Next-generation sequencing of the amplified sgRNA library has been described previously (*82*). Amplification was performed using Phusion High-Fidelity PCR Master Mix with HF Buffer (New England Biolabs, catalog no. M0530), with the following conditions: 95°C 5 min, [98°C 20 s, 60°C 15 s, 72°C 15 s] × 18 cycles, followed by 72°C for 1 min for extension. Then, PCR amplicons were purified on AMPure beads (Beckman Coulter).

MAGeCK Analysis

We analyzed the sgRNA read count data from the CRISPR screen experiments using the MAGeCK package. The MAGeCK count command was used to preprocess and normalize the data for controls and for the different treatment groups. Then, the MAGeCK mle command was used to perform gene essentiality analysis based on the design matrix of treatment versus control, taking into account the nontargeting control guide. The MAGeCK output file lists the gene summary including ranking of enriched genes. Metascape (*83*) was used for pathway analysis.

Microscopy and image analysis

Time-lapse microscopy was performed using a Yokogawa CSU-X1 spinning disk mounted on an inverted Nikon Eclipse Ti microscope equipped with dual Andor iXon EMCCD cameras and a climate controlled motorized x-y or with the Zeiss CR7 Live/High content equipped

with the Prime 95B camera with control CO_2 and temperature. Animals were only included for imaging and analysis if expression of all transgenes could be identified. Images were acquired using NIS-Elements (Nikon) or Zen Blue software, blinded, and processed using Imaris (Bitplane). Specimens were mounted in 0.4% low-melting-point agarose with tricaine (0.16 mg/ml) in glass-bottom dishes and covered with E3 media containing tricaine (0.16 mg/ml).

Flow cytometry

For embryonic stainings, 3-dpf tails were chopped with a razor blade in cold PBS and then incubated in Liberase (Roche) for 30 min at 37°C before filtering the dissociated cells through a 40-μm filter and transferring to PBS–1% FBS solution.

To collect adult kidney marrow, adult zebrafish (4 to 6 months-old) were anesthetized with fresh tricaine (0.02%) in E3 fish water and dissected under a Leica MZ75 light microscope. The kidney marrow was transferred into 1.5-ml microtube containing cold PBS (Gibco) supplemented with 2% FBS (Gemini Bio-Products) and 1 USP units/ml heparin (Sigma), and then mechanically dissociated by pipetting. After single-cell suspension, the sample was passed through a 40-μm nylon mesh 5 to 10 min before FACS acquisition and stained with Zombie Dye (BioLegend) for cell viability detection.

CellROX Deep Red (Invitrogen, catalog no. C10422), Annexin V-FITC (BD Biosciences), JC-1 (Biotium, catalog no. 30001), Mitotracker CMX, and zymosan staining were performed according to the manufacturers' instructions.

The following antibodies were used for flow cytometry: anti-human B2M (APC/Fire750, BioLegend, clone 2M2, catalog no. A17082A), anti-mouse F480 (AF594, BioLegend, clone BM8, catalog no. 123140), anti-human CD34 (PeCy7, BD Bioscience, clone 8G12, catalog no. 348791), Lineage selection kit (Pacific Blue, BioLegend, CD3, clone 17A2; anti-mouse Ly-6G/Ly-6C, clone RB6-8C5; anti-mouse CD11b, clone M1/70; anti-mouse CD45R/B220, clone RA3-6B2; anti-mouse TER-119/erythroid cells, catalog no. 133310), anti-mouse CD117 (APC, clone 104D2, BioLegend, S18020A), Sca-1 (PeCy7, BioLegend, clone D7, catalog no. 108113).

Flow cytometric analysis was performed on a BD FACSFortessa or BD FACS symphony flow cytometer. Data were analyzed with FlowJo software version 10.

Embryo generation for chemical screen validation

For chemical screen validation, *Casper* fish were spawned in iSpawns for 15 min, and embryos were collected into embryo medium (E3) and cleaned using a water gradient for 48 hours. At 2 dpf, the viable embryos were sorted and kept at 25 to 30 embryos per well in six-well plates and treated with the 22 Calr inducer candidates.

Zebrabow color labeling

At 24 hpf, embryos were transferred to six-well plates at a density of 25 to 35 embryos per well and treated with 15 μM 4-hydroxytamoxifen (4-OHT) for 3 to 5 hours in the dark at 28.5°C (*31*). Zebrabow analysis was conducted using zbow software. Only zebrafish with >75% recombination efficiency were processed.

Drug treatment

Drugs were added to embryo E3 media in six-well plates with 20 to 30 embryos per well at 48 hpf and incubated for 24 hours. Inducers (see data S1) were added at a concentration of 50 μM. DPI (Sigma) was added to embryos at a concentration of 100 μM. VAS2870 (Sigma) was added at a concentration of 20 μM. CM272 (Cayman Chemicals, catalog no. 25948) was added at a concentration of 2 μM. Poly I:C (Sigma) and CU-CPT4a (Cayman Chemicals, catalog no. 30951) were added at a concentration of 50 μM each.

Morpholino injections

Tlr3 morpholino was selected from the *zfin* database (*84*) and purchased at GeneTools. It was resuspended to 300 μM in nuclease-free water, heated to 65°C for 5 min, and kept at room temperature. Embryos were injected into the yolk at the one-cell stage with 10 ng of morpholino. Morpholino sequences are listed in data S3.

Liposome injection

Zebrafish embryos were dechorionated and anesthetized with tricaine (0.16 mg/ml) on flat agarose disks. Approximately 1.5 nl of liposomes were loaded with either clodronate or PBS.

Zebrafish EdU Labeling

Embryonic circulation was injected at 3 dpf with 1 nl of 500 μM EdU. Embryos were kept at 4°C for 1 hour, fixed in 4% paraformaldehyde for 1 hour, permeabilized with 0.1% Triton X-100 for 20 min at room temperature, and labeled with Alexa Fluor 647 using the Click-iT reaction (Thermo Fisher) for 30 min according to the manufacturer's instructions. Embryos were washed with PBS plus 0.5% Triton X-100 and blocked for 1 hour in 10% normal goat serum, 0.5% bovine serum albumin, 0.5% Triton X-100. Samples were incubated in rat anti-mCherry Alexa Fluor 594 (Invitrogen M11240, 1:200, RRID:AB_2536614) for 1 hour at room temperature and washed five times with PBS plus 0.5% Triton X-100.

dsRNA staining

Embryos were dissociated in 0.5 mg/ml Liberase TM (Roche) solution for 30 min at 37°C, then dissociated by pipetting and resuspended in FACS buffer (PBS, 1% FBS, 1 mM EDTA). Cells were then fixed in 4% paraformaldehyde at 4°C and permeabilized in PBS with 0.1% Tween v/v (PBS-T) for 30 min on ice. Cells were washed twice with FACS buffer and incubated overnight with dsRNA anti-mouse J2 mAb (Millipore, catalog no. MABE1134) at a concentration of 1/100. The next day, three washes were performed in the FACS buffer after incubation with a secondary antibody (goat anti-mouse IgG1 AF488) for 30 min at room temperature.

CRISPR-Cas9 mutagenesis

Target selection for CRISPR-Cas9–mediated mutagenesis was performed using CHOPCHOP (*85*). The selected sgRNA (data S3) having a GC content <55%, mismatches (MM) self-complementarity = 0, MM0 ≤ 1, MM1 ≤ 1, MM2 ≤ 1, MM3 ≤ 1. The sgRNA templates were generated using the protocol described by Gagnon *et al.* (*86*) using the mMESSAGE mMACHINETM SP6 transcription kit (Invitrogen, AM1340). The guide RNAs (gRNAs) were validated using T7 endonuclease I assay in 72-hpf embryos.

Editing efficiency was further validated by deep sequencing of PCR amplicons. In brief, genomic DNA from zebrafish tissue was extracted with DNeasy blood and tissue kit (Qiagen, catalog no. 69506). The CRISPR loci of the targeted genes were amplified using the primers above and barcoded with the Illumina NGS adapter. Amplification was performed using Phusion High-Fidelity PCR Master Mix with HF Buffer (New England Biolabs, catalog no. M0530) under the following conditions: 98°C for 3 min, 98°C for 10 s, time for annealing for 10 s, and 72°C for 10 s × 35 cycles, and then 72°C for 5 min. Temperature of annealing was 63°C]. Then, PCR amplicons were purified on PCR purification kit columns before sequencing.

sgRNA and Cas9 injections

The gRNAs were resuspended to 1 ng/μL in nuclease-free water, and protein TrueCut Cas9 protein (Thermo Fisher, catalog no. A36498) was added to the solution, which was kept at room temperature for 5 min. Embryos were injected at the one-cell stage with 0.2 ng of gRNA.

Mutagenesis analysis

For mutagenesis analysis, the sequencing reads were first trimmed for quality and aligned to the GRCz11/danRer11 assembly using Bowtie2 (*87*) using the very-sensitive setting. Mutations were quantified with R software CrispRVariants-version 1.20 (*88*) using a minimum read count of 20. The R version used in this analysis was 4.1.0 (2021-05-18).

Single-cell RNA-seq analysis

REs sequences from *Danio rerio* were obtained from RepBase. Sequencing data from Wattrus *et al.* (*6*) were then aligned to the RE

library using Bowtie2 (*87*). Reads uniquely aligned to the RE were then identified by filtering for mapping qualities >5, and the number of reads aligning to each RE was counted using count features. To identify differentially expressed REs, the DESeq2 R package (*43*) was used.

mRNA synthesis and CD34 overexpression

For the overexpression of human *ERV* the respective cDNA was amplified from CD34 cells with PCR and cloned into pJET1.2/blunt cloning vector (CloneJET PCR Cloning Kit, Thermoscientific, catalog no. K1232). The constructs were linearized and used as templates for in vitro mRNA synthesis (T7 mMESSAGE mMACHINE kit, Ambion, catalog no. AM1344). Cells were electroporated with Lonza P3 primary solution using the DZ100 program. The *ERV* genomic location was retrieved from the *Dfam* database (*89*).

RNA extraction

Embryos (3 dpf) were lysed in TRIzol (Invitrogen, catalog no. 15596026) by mechanical force. To isolate RNA, chloroform was added, followed by extraction and precipitation of the aqueous phase using 5 μg of ribonuclease (RNase)–free glycogen and 0.25 ml of isopropanol. The supernatant was discarded, and the pellet was washed twice in 80% ethanol and then dissolved in 10 μl of H_2O.

Reverse transcription qPCR

RNA (500 ng) was reversely transcribed into complementary DNA using Superscript VIlo RT (Thermo Fisher Scientific). Reverse transcription (RT)-qPCR was performed using SYBR Green Master Mix (Roche, catalog no. 4309155); the mixture contained 6.25 μl of SYBR, 0.75 μl of primers (forward and reverse, 300 nM), and 4.5 μl of H_2O.

Mouse cell culture

Mouse BMDMs were generated from bone marrow precursors by standard macrophage-colony stimulating factor (M-CSF), PeproTech culture. The tibia and femora where marrow content was fluxed was flushed with cold PBS. The bone marrow suspension was passed through a 40-μm filter and pelted in a centrifuge at 500*g* for 5 min. Cells were counted and resuspended at 2×10^6 cells/ml with 10% FBS, 1% pen/strep–IMDM, and 20 ng/ml M-CSF (PeproTech). The cell suspension was plated on a six-well plate and incubated at 37°C under 5% CO_2 (day 0). On day 3, 5 ml of fresh medium containing 20 ng/ml M-CSF was added on top of the pre-existing medium. Cells were harvested with cold PBS supplemented with 1 mM EDTA at day 5 of differentiation.

For three-dimensional co-culture, BMDMs were seeded at a concentration of 1×10^5 cells/ml with autologous sorted HSPCs (LSK^+) in 40% Matrigel in a 96-well glass-bottom plate. After adding the cells into the Matrigel solution, the plates were centrifuged for 3 min at 75*g* and 4°C to bring the macrophages and HSPCs into the same focal plane for imaging. Plates were then incubated at 37°C for 30 min to ensure complete polymerization of the gel. Samples were then left at room temperature for 10 min before 200 μl of 10% IMDM medium was added on top of the Matrigel. Each well was imaged in 10-min intervals for 2 hours using the Zeiss AiryScan confocal microscope or the Yokogawa CSU-X1 spinning-disk microscope.

Macrophage line RAW-274 chemotaxis

To analyze the inducer-driven macrophage migration toward the chemoattractant (LPS, 50 ng/μL), we used under-agarose chemotaxis assays (*12*). In brief, agarose gels were cast into 35 × 10-mm tissue culture dishes (Corning). After gel polymerization, wells with a diameter of 4 mm were punched into the gel in ~3-mm distances using a cartoon template. Twelve wells were punched in the agarose gel per dish; the left one was loaded with the inducer-treated or LPS-treated Raw274. The right well was loaded with the chemoattractant. The cells were previously labeled with CellTracker Red following the manufacturer's recommendations.

Human $CD34^+$ RNA-seq analysis

Human bone marrow single-cell RNA-seq data were downloaded from the DISCO database (*50*). The cells annotated as HSCs were analyzed for the expression of ISG15. HSCs with expression of at least one unique molecular identifier (UMI) of ISG15 were divided into ISG15-low and ISG15-high (i.e., upper quartile of normalized ISG15 expression) cells and analyzed for B2M expression. The gene expressions were normalized by total UMI per cell, multiplied by a scale factor of 10,000 and log transformed. Linear mixed-effects analysis was performed using the lme4 package (v.1.2-1). ISG15 status was entered as the fixed effect and subjects as random effects. *P* values were obtained by likelihood ratio tests of the full model with the fixed effect against the model without the fixed effect. For the correlation of ISG15 expression and TE transcripts, single-cell RNA-seq fastq files of bone marrow $CD34^+$ cells from individuals with *Calr*-mutated essential thrombocythemia (*90*) were processed using Cell Ranger (v. 7.1.0) using chm13v2.0.fa and T2T_CHM13_v2_rmsk_TE.gtf files from T2T-CHM13v2.0 (*91*) to annotate the aligned reads for TE. HSCs with at least one transcript expression of ISG15 were included to determine the correlation of ISG15 expression versus TE expression (normalized by total UMI per cell; Pearson's correlation).

In vivo Edu staining

Mice were retro-orbitally injected with 1× EdU (500 μM) and DL-PPMP (0.8 mg/kg, Cayman Chemicals, catalog no. 17236) or DMSO. After 24 hours, they were anesthetized by vaporized isoflurane (3 to 4% for induction and 1 to 2% for maintenance) and sacrificed by cervical dislocation. The bone marrow was isolated from pooled femora and tibia by flushing them with cold PBS containing 2% fetal calf serum. Lysis of erythrocytes was performed using ACK lysing buffer, and the remaining cells were stained with Zombie dye for viability, anti-Edu as described above anti-B2M (APC-Fire700, 2M2). Data were acquired with a FACSAria Fusion II flow cytometer (BD Biosciences). A list of antibody panel repertoires is provided in the supplementary materials.

Statistical analysis

Graphs and statistical analyses were done with Prism (GraphPad) and Rstudio software. For all graphs, error bars indicate mean ± SEM. *P* values were obtained with two-tailed Student's *t* test, Mann-Whitney *U* test, or one-way ANOVAs for all analyses as indicated. Sample sizes were chosen on the basis of sample availability, and power calculations were determined from preliminary observations to detect a change of at least 33% with an α of 0.05 and a β of 0.8. For all experiments except Zebrabow color labeling, a randomized set of embryos from a mixture of clutches was split into control and perturbation conditions. All experiments were performed at least twice.

REFERENCES AND NOTES

1. D. V. Krysko, P. Vandenabeele, *Phagocytosis of Dying Cells: From Molecular Mechanisms to Human Diseases* (Springer, 2009). doi: 10.1007/978-1-4020-9293-0
2. S. Arandjelovic, K. S. Ravichandran, Phagocytosis of apoptotic cells in homeostasis. *Nat. Immunol.* **16**, 907–917 (2015). doi: 10.1038/ni.3253; pmid: 26287597
3. S. M. Kelley, K. S. Ravichandran, Putting the brakes on phagocytosis: "don't-eat-me" signaling in physiology and disease. *EMBO Rep.* **22**, e52564 (2021). doi: 10.15252/embr.202152564; pmid: 34041845
4. F. A. Arosa, O. de Jesus, G. Porto, A. M. Carmo, M. de Sousa, Calreticulin is expressed on the cell surface of activated human peripheral blood T lymphocytes in association with major histocompatibility complex class I molecules. *J. Biol. Chem.* **274**, 16917–16922 (1999). doi: 10.1074/jbc.274.24.16917; pmid: 10358038
5. J. Y. Bertrand *et al*., Haematopoietic stem cells derive directly from aortic endothelium during development. *Nature* **464**, 108–111 (2010). doi: 10.1038/nature08738; pmid: 20154733
6. S. J. Wattrus *et al*., Quality assurance of hematopoietic stem cells by macrophages determines stem cell clonality. *Science* **377**, 1413–1419 (2022). doi: 10.1126/science.abo4837; pmid: 36137040
7. P. Storz, Forkhead homeobox type O transcription factors in the responses to oxidative stress. *Antioxid. Redox Signal.* **14**, 593–605 (2011). doi: 10.1089/ars.2010.3405; pmid: 20618067
8. P. Niethammer, C. Grabher, A. T. Look, T. J. Mitchison, A tissue-scale gradient of hydrogen peroxide mediates rapid wound detection in zebrafish. *Nature* **459**, 996–999 (2009). doi: 10.1038/nature08119; pmid: 19494811
9. K. F. Cho *et al*., Split-TurboID enables contact-dependent proximity labeling in cells. *Proc. Natl. Acad. Sci. U.S.A.* **117**, 12143–12154 (2020). doi: 10.1073/pnas.1919528117; pmid: 32424107
10. S. Deghou *et al*., CART-a chemical annotation retrieval toolkit. *Bioinformatics* **32**, 2869–2871 (2016). doi: 10.1093/bioinformatics/btw233; pmid: 27256313
11. O. J. Tamplin *et al*., Hematopoietic stem cell arrival triggers dynamic remodeling of the perivascular niche. *Cell* **160**, 241–252 (2015). doi: 10.1016/j.cell.2014.12.032; pmid: 25594182

12. B. Heit, P. Kubes, Measuring chemotaxis and chemokinesis: The under-agarose cell migration assay. *Sci. STKE* **2003**, PL5 (2003). doi: 10.1126/stke.2003.170.pl5; pmid: 12591998
13. O. Shalem *et al*., Genome-scale CRISPR-Cas9 knockout screening in human cells. *Science* **343**, 84–87 (2014). doi: 10.1126/science.1247005; pmid: 24336571
14. C.-Y. Yu, Y.-W. Hsu, C.-L. Liao, Y.-L. Lin, Flavivirus infection activates the XBP1 pathway of the unfolded protein response to cope with endoplasmic reticulum stress. *J. Virol.* **80**, 11868–11880 (2006). doi: 10.1128/JVI.00879-06; pmid: 16987981
15. J. Kwon, H. Choi, C. Han, A Dual Role of DDX3X in dsRNA-Derived Innate Immune Signaling. *Front. Mol. Biosci.* **9**, 912727 (2022). doi: 10.3389/fmolb.2022.912727; pmid: 35874614
16. S. Chattopadhyay, G. C. Sen, dsRNA-activation of TLR3 and RLR signaling: Gene induction-dependent and independent effects. *J. Interferon Cytokine Res.* **34**, 427–436 (2014). doi: 10.1089/jir.2014.0034; pmid: 24905199
17. K. Cheng, X. Wang, H. Yin, Small-molecule inhibitors of the TLR3/dsRNA complex. *J. Am. Chem. Soc.* **133**, 3764–3767 (2011). doi: 10.1021/ja111312h; pmid: 21355588
18. J. R. Perlin, A. Sporrij, L. I. Zon, Blood on the tracks: Hematopoietic stem cell-endothelial cell interactions in homing and engraftment. *J. Mol. Med.* **95**, 809–819 (2017). doi: 10.1007/s00109-017-1559-8; pmid: 28702683
19. P. Zhang *et al*., IPS-1 plays an essential role in dsRNA-induced stress granule formation by interacting with PKR and promoting its activation. *J. Cell Sci.* **127**, 2471–2482 (2014). pmid: 24659800
20. J. Lamb *et al*., The Connectivity Map: Using gene-expression signatures to connect small molecules, genes, and disease. *Science* **313**, 1929–1935 (2006). doi: 10.1126/science.1132939; pmid: 17008526
21. J. Sun, D. J. Leahy, P. B. Kavathas, Interaction between CD8 and major histocompatibility complex (MHC) class I mediated by multiple contact surfaces that include the alpha 2 and alpha 3 domains of MHC class I. *J. Exp. Med.* **182**, 1275–1280 (1995). doi: 10.1084/jem.182.5.1275; pmid: 7595198
22. A. A. Barkal *et al*., Engagement of MHC class I by the inhibitory receptor LILRB1 suppresses macrophages and is a target of cancer immunotherapy. *Nat. Immunol.* **19**, 76–84 (2018). doi: 10.1038/s41590-017-0004-z; pmid: 29180808
23. C. C. Chang *et al*., Tolerization of dendritic cells by T(S) cells: The crucial role of inhibitory receptors ILT3 and ILT4. *Nat. Immunol.* **3**, 237–243 (2002). doi: 10.1038/ni760; pmid: 11875462
24. Y. Liu *et al*., Emerging phagocytosis checkpoints in cancer immunotherapy. *Signal Transduct. Target. Ther.* **8**, 104 (2023). doi: 10.1038/s41392-023-01365-z; pmid: 36882399
25. J. L. Stafford, E. Bengtén, L. Du Pasquier, N. W. Miller, M. Wilson, Channel catfish leukocyte immune-type receptors contain a putative MHC class I binding site. *Immunogenetics* **59**, 77–91 (2007). doi: 10.1007/s00251-006-0169-3; pmid: 17149620
26. L. Storm, J. Bruijnesteijn, N. G. de Groot, R. E. Bontrop, The genomic organization of the LILR region remained largely conserved throughout primate evolution: Implications for health and disease. *Front. Immunol.* **12**, 716289 (2021). doi: 10.3389/fimmu.2021.716289; pmid: 34737739
27. B. H. Koller, P. Marrack, J. W. Kappler, O. Smithies, Normal development of mice deficient in beta 2M, MHC class I proteins, and CD8+ T cells. *Science* **248**, 1227–1230 (1990). doi: 10.1126/science.2112266; pmid: 2112266
28. M. Zijlstra *et al*., β 2-microglobulin deficient mice lack CD4-8+ cytolytic T cells. *Nature* **344**, 742–746 (1990). doi: 10.1038/344742a0; pmid: 2139497
29. J. Sun *et al*., Clonal dynamics of native haematopoiesis. *Nature* **514**, 322–327 (2014). doi: 10.1038/nature13824; pmid: 25296256
30. V. G. Sankaran, J. S. Weissman, L. I. Zon, Cellular barcoding to decipher clonal dynamics in disease. *Science* **378**, eabm5874 (2022). doi: 10.1126/science.abm5874; pmid: 36227997
31. J. Henninger *et al*., Clonal fate mapping quantifies the number of haematopoietic stem cells that arise during development. *Nat. Cell Biol.* **19**, 17–27 (2017). doi: 10.1038/ncb3444; pmid: 27870830
32. S. Avagyan *et al*., Resistance to inflammation underlies enhanced fitness in clonal hematopoiesis. *Science* **374**, 768–772 (2021). doi: 10.1126/science.aba9304; pmid: 34735227
33. S. Doyle *et al*., IRF3 mediates a TLR3/TLR4-specific antiviral gene program. *Immunity* **17**, 251–263 (2002). doi: 10.1016/S1074-7613(02)00390-4; pmid: 12354379
34. S. J. P. Gobin, P. Biesta, P. J. Van den Elsen, Regulation of human beta 2-microglobulin transactivation in hematopoietic cells. *Blood* **101**, 3058–3064 (2003). doi: 10.1182/blood-2002-09-2924; pmid: 12480693
35. C. Caiazza *et al*., The lack of STING impairs the MHC-I dependent antigen presentation and JAK/STAT signaling in murine macrophages. *Int. J. Mol. Sci.* **23**, 14232 (2022). doi: 10.3390/ijms232214232; pmid: 36430709
36. C. E. McCoy, S. Carpenter, E. M. Pålsson-McDermott, L. J. Gearing, L. A. J. O'Neill, Glucocorticoids inhibit IRF3 phosphorylation in response to Toll-like receptor-3 and -4 by targeting TBK1 activation. *J. Biol. Chem.* **283**, 14277–14285 (2008). doi: 10.1074/jbc.M709731200; pmid: 18356163
37. Y.-C. Perng, D. J. Lenschow, ISG15 in antiviral immunity and beyond. *Nat. Rev. Microbiol.* **16**, 423–439 (2018). doi: 10.1038/s41579-018-0020-5; pmid: 29769653
38. C. Langevin *et al*., Zebrafish ISG15 exerts a strong antiviral activity against RNA and DNA viruses and regulates the interferon response. *J. Virol.* **87**, 10025–10036 (2013). doi: 10.1128/JVI.01294-12; pmid: 23824820
39. K. M. Balla, M. C. Rice, J. A. Gagnon, N. C. Elde, Linking virus discovery to immune responses visualized during zebrafish infections. *Curr. Biol.* **30**, 2092–2103.e5 (2020). doi: 10.1016/j.cub.2020.04.031; pmid: 32413307
40. S. Lefkopoulos *et al*., Repetitive elements trigger RIG-I-like receptor signaling that regulates the emergence of hematopoietic stem and progenitor cells. *Immunity* **53**, 934–951.e9 (2020). doi: 10.1016/j.immuni.2020.10.007; pmid: 33159854
41. T. Clapes *et al*., Chemotherapy-induced transposable elements activate MDA5 to enhance haematopoietic regeneration. *Nat. Cell Biol.* **23**, 704–717 (2021). doi: 10.1038/s41556-021-00707-9; pmid: 34253898
42. Y. Chen, J. Lin, Y. Zhao, X. Ma, H. Yi, Toll-like receptor 3 (TLR3) regulation mechanisms and roles in antiviral innate immune responses. *J. Zhejiang Univ. Sci. B* **22**, 609–632 (2021). doi: 10.1631/jzus.B2000808; pmid: 34414698
43. Y. Jin, O. H. Tam, E. Paniagua, M. Hammell, TEtranscripts: A package for including transposable elements in differential expression analysis of RNA-seq datasets. *Bioinformatics* **31**, 3593–3599 (2015). doi: 10.1093/bioinformatics/btv422; pmid: 26206304
44. H. A. Rutherford *et al*., A zebrafish reporter line reveals immune and neuronal expression of endogenous retrovirus. *Dis. Model. Mech.* **15**, dmm048921 (2022). doi: 10.1242/dmm.048921; pmid: 35142349
45. E. San José-Enériz *et al*., Discovery of first-in-class reversible dual small molecule inhibitors against G9a and DNMTs in hematological malignancies. *Nat. Commun.* **8**, 15424 (2017). doi: 10.1038/ncomms15424; pmid: 28548080
46. K. B. Chiappinelli *et al*., Inhibiting DNA methylation causes an interferon response in cancer via dsRNA including endogenous retroviruses. *Cell* **169**, 361 (2017). doi: 10.1016/j.cell.2017.03.036; pmid: 28388418
47. C. Haggerty *et al*., Dnmt1 has de novo activity targeted to transposable elements. *Nat. Struct. Mol. Biol.* **28**, 594–603 (2021). doi: 10.1038/s41594-021-00603-8; pmid: 34140676
48. H. Ono, F. Figueroa, C. O'hUigin, J. Klein, Cloning of the β 2-microglobulin gene in the zebrafish. *Immunogenetics* **38**, 1–10 (1993). doi: 10.1007/BF00216384; pmid: 8462988
49. D. C. Chapman, D. B. Williams, ER quality control in the biogenesis of MHC class I molecules. *Semin. Cell Dev. Biol.* **21**, 512–519 (2010). doi: 10.1016/j.semcdb.2009.12.013; pmid: 20044014
50. M. Li *et al*., DISCO: A database of Deeply Integrated human Single-Cell Omics data. *Nucleic Acids Res.* **50**, D596–D602 (2022). doi: 10.1093/nar/gkab1020; pmid: 34791375
51. C. Christodoulou *et al*., Live-animal imaging of native haematopoietic stem and progenitor cells. *Nature* **578**, 278–283 (2020). doi: 10.1038/s41586-020-1971-z; pmid: 32025033
52. Y. Zhang *et al*., PR-domain-containing Mds1-Evi1 is critical for long-term hematopoietic stem cell function. *Blood* **118**, 3853–3861 (2011). doi: 10.1182/blood-2011-02-334680; pmid: 21666053
53. C. A. Buttler, E. B. Chuong, Emerging roles for endogenous retroviruses in immune epigenetic regulation. *Immunol. Rev.* **305**, 165–178 (2022). doi: 10.1111/imr.13042; pmid: 34816452
54. E. Russ, S. Iordanskiy, Endogenous retroviruses as modulators of innate immunity. *Pathogens* **12**, 162 (2023). doi: 10.3390/pathogens12020162; pmid: 36839434
55. S. Srinivasachar Badarinarayan *et al*., HIV-1 infection activates endogenous retroviral promoters regulating antiviral gene expression. *Nucleic Acids Res.* **48**, 10890–10908 (2020). doi: 10.1093/nar/gkaa832; pmid: 33021676
56. L. Bogdan, L. Barreiro, G. Bourque, Transposable elements have contributed human regulatory regions that are activated upon bacterial infection. *Philos. Trans. R. Soc. Lond. B Biol. Sci.* **375**, 20190332 (2020). doi: 10.1098/rstb.2019.0332; pmid: 32075553
57. J. Ochando, W. J. M. Mulder, J. C. Madsen, M. G. Netea, R. Duivenvoorden, Trained immunity - basic concepts and contributions to immunopathology. *Nat. Rev. Nephrol.* **19**, 23–37 (2023). doi: 10.1038/s41581-022-00633-5; pmid: 36253509
58. M. G. Manz, S. Boettcher, Emergency granulopoiesis. *Nat. Rev. Immunol.* **14**, 302–314 (2014). doi: 10.1038/nri3660; pmid: 24751955
59. S. Paudel, L. Ghimire, L. Jin, D. Jeansonne, S. Jeyaseelan, Regulation of emergency granulopoiesis during infection. *Front. Immunol.* **13**, 961601 (2022). doi: 10.3389/fimmu.2022.961601; pmid: 36148240
60. Y. Katahira *et al*., Increased granulopoiesis in the bone marrow following Epstein-Barr virus infection. *Sci. Rep.* **9**, 13445 (2019). doi: 10.1038/s41598-019-49937-w; pmid: 31530932
61. J. G. Donaldson, D. B. Williams, Intracellular assembly and trafficking of MHC class I molecules. *Traffic* **10**, 1745–1752 (2009). doi: 10.1111/j.1600-0854.2009.00979.x; pmid: 19761542
62. S. Apcher, B. Manoury, R. Fåhraeus, The role of mRNA translation in direct MHC class I antigen presentation. *Curr. Opin. Immunol.* **24**, 71–76 (2012). doi: 10.1016/j.coi.2012.01.007; pmid: 22341517
63. J. G. Sambrook, F. Figueroa, S. Beck, A genome-wide survey of Major Histocompatibility Complex (MHC) genes and their paralogues in zebrafish. *BMC Genomics* **6**, 152 (2005). doi: 10.1186/1471-2164-6-152; pmid: 16271140
64. E. W. Hewitt, The MHC class I antigen presentation pathway: Strategies for viral immune evasion. *Immunology* **110**, 163–169 (2003). doi: 10.1046/j.1365-2567.2003.01738.x; pmid: 14511229
65. Y. Demerdash, B. Kain, M. A. G. Essers, K. Y. King, Yin and Yang: The dual effects of interferons on hematopoiesis. *Exp. Hematol.* **96**, 1–12 (2021). doi: 10.1016/j.exphem.2021.02.002; pmid: 33571568
66. M. A. G. Essers *et al*., IFNalpha activates dormant haematopoietic stem cells in vivo. *Nature* **458**, 904–908 (2009). doi: 10.1038/nature07815; pmid: 19212321
67. E. M. Pietras *et al*., Re-entry into quiescence protects hematopoietic stem cells from the killing effect of chronic exposure to type I interferons. *J. Exp. Med.* **211**, 245–262 (2014). doi: 10.1084/jem.20131043; pmid: 24493802
68. P. G. Kim *et al*., Interferon-α signaling promotes embryonic HSC maturation. *Blood* **128**, 204–216 (2016). doi: 10.1182/blood-2016-01-689281; pmid: 27095787
69. M. A. Garrido *et al*., HLA class I alterations in breast carcinoma are associated with a high frequency of the loss of heterozygosity at chromosomes 6 and 15. *Immunogenetics* **70**, 647–659 (2018). doi: 10.1007/s00251-018-1074-2; pmid: 30145665
70. R. Squire, C. L. Fowler, S. P. Brooks, G. A. Rich, D. R. Cooney, The relationship of class I MHC antigen expression to stage IV-S disease and survival in neuroblastoma. *J. Pediatr. Surg.* **25**, 381–386 (1990). doi: 10.1016/0022-3468(90)90375-J; pmid: 2329454
71. T. Hanagiri *et al*., Prognostic implications of human leukocyte antigen class I expression in patients who underwent surgical resection for non-small-cell lung cancer. *J. Surg. Res.* **181**, e57–e63 (2013). doi: 10.1016/j.jss.2012.07.029; pmid: 22878150
72. S. Sen Santara *et al*., The NK cell receptor NKp46 recognizes ecto-calreticulin on ER-stressed cells. *Nature* **616**, 348–356 (2023). doi: 10.1038/s41586-023-05912-0; pmid: 37020026
73. M. Tobiasson *et al*., Comprehensive mapping of the effects of azacitidine on DNA methylation, repressive/permissive histone marks and gene expression in primary cells from patients with MDS and MDS-related disease. *Oncotarget* **8**, 28812–28825 (2017). doi: 10.18632/oncotarget.15807; pmid: 28427179
74. R. Edlin *et al*., Azacitidine for the treatment of myelodysplastic syndrome, chronic myelomonocytic leukaemia and acute myeloid leukaemia. *Health Technol. Assess.* **14**, 69–74 (2010). doi: 10.3310/hta14Suppl1-10; pmid: 20507806
75. C. D. DiNardo *et al*., Azacitidine and venetoclax in previously untreated acute myeloid leukemia. *N. Engl. J. Med.* **383**, 617–629 (2020). doi: 10.1056/NEJMoa2012971; pmid: 32786187

76. C. P. Rodrigues, M. Shvedunova, A. Akhtar, Epigenetic regulators as the gatekeepers of hematopoiesis. *Trends Genet.* 10.1016/j.tig.2020.09.015 (2020). doi: 10.1016/j.tig.2020.09.015; pmid: 34756331
77. A. R. Colombo, T. Triche Jr., G. Ramsingh, Transposable element expression in acute myeloid leukemia transcriptome and prognosis. *Sci. Rep.* **8**, 16449 (2018). doi: 10.1038/s41598-018-34189-x; pmid: 30401833
78. R. M. White *et al*., Transparent adult zebrafish as a tool for in vivo transplantation analysis. *Cell Stem Cell* **2**, 183–189 (2008). doi: 10.1016/j.stem.2007.11.002; pmid: 18371439
79. C. Mosimann *et al*., Chamber identity programs drive early functional partitioning of the heart. *Nat. Commun.* **6**, 8146 (2015). doi: 10.1038/ncomms9146; pmid: 26306682
80. F. Ellett, L. Pase, J. W. Hayman, A. Andrianopoulos, G. J. Lieschke, mpeg1 promoter transgenes direct macrophage-lineage expression in zebrafish. *Blood* **117**, e49–e56 (2011). doi: 10.1182/blood-2010-10-314120; pmid: 21084707
81. N. E. Sanjana, O. Shalem, F. Zhang, Improved vectors and genome-wide libraries for CRISPR screening. *Nat. Methods* **11**, 783–784 (2014). doi: 10.1038/nmeth.3047; pmid: 25075903
82. J. Joung *et al*., Genome-scale CRISPR-Cas9 knockout and transcriptional activation screening. *Nat. Protoc.* **12**, 828–863 (2017). doi: 10.1038/nprot.2017.016; pmid: 28333914
83. Y. Zhou *et al*., Metascape provides a biologist-oriented resource for the analysis of systems-level datasets. *Nat. Commun.* **10**, 1523 (2019). doi: 10.1038/s41467-019-09234-6; pmid: 30944313
84. F. Alcaraz-Pérez, V. Mulero, M. L. Cayuela, Application of the dual-luciferase reporter assay to the analysis of promoter activity in Zebrafish embryos. *BMC Biotechnol.* **8**, 81 (2008). doi: 10.1186/1472-6750-8-81; pmid: 18954456
85. K. Labun *et al*., CHOPCHOP v3: Expanding the CRISPR web toolbox beyond genome editing. *Nucleic Acids Res.* **47**, W171–W174 (2019). doi: 10.1093/nar/gkz365; pmid: 31106371
86. J. A. Gagnon *et al*., Efficient mutagenesis by Cas9 protein-mediated oligonucleotide insertion and large-scale assessment of single-guide RNAs. *PLOS ONE* **9**, e98186 (2014). doi: 10.1371/journal.pone.0098186; pmid: 24873830
87. B. Langmead, S. L. Salzberg, Fast gapped-read alignment with Bowtie 2. *Nat. Methods* **9**, 357–359 (2012). doi: 10.1038/nmeth.1923; pmid: 22388286
88. H. Lindsay *et al*., CrispRVariants charts the mutation spectrum of genome engineering experiments. *Nat. Biotechnol.* **34**, 701–702 (2016). doi: 10.1038/nbt.3628; pmid: 27404876
89. R. Hubley *et al*., The Dfam database of repetitive DNA families. *Nucleic Acids Res.* **44**, D81–D89 (2016). doi: 10.1093/nar/gkv1272; pmid: 26612867
90. A. S. Nam *et al*., Somatic mutations and cell identity linked by Genotyping of Transcriptomes. *Nature* **571**, 355–360 (2019). doi: 10.1038/s41586-019-1367-0; pmid: 31270458
91. S. Aganezov *et al*., A complete reference genome improves analysis of human genetic variation. *Science* **376**, eabl3533 (2022). doi: 10.1126/science.abl3533; pmid: 35357935

ACKNOWLEDGMENTS

We gratefully thank the members of the Zon lab, the Harvard Stem Cell & Regenerative Biology (HSCRB) Department, Boston Children's Hospital staff, the Harvard Bauer flow cytometry core, the Harvard Bauer sequencing core, the HCBI core, the HSCRB veterinarians and animal caretakers (I. Adatto, S. Freyer, and H. Nations), A. Noemi for providing the zfLTR5 plasmid, N. C. C. Elde for providing the isg15-GFP zebrafish and colleagues for critical reading of the manuscript and sharing reagents. We are also grateful to the Edward P. Evans Foundation and the Alexs Lemonade Stand Fund for their support. Some figures were created with BioRender.com. **Funding:** This work was supported by the National Institutes of Health (grant 5T32HL007574-40 to C.P.R.; grants P01HL131477, P01HL032262, U54DK110805, R24DK092760, R24OD017870, U01HL134812, and R01HL144780-01 to L.I.Z.; Director's Early Independence Award DP5 OD029619 to A.S.N.; and National Heart Lung and Blood Institute Grant R01 HL167139 to A.S.N.); the Edward P. Evans Foundation (L.I.Z.); the Crazy 8 Initiative Award Program (L.I.Z.); Alex's Lemonade Stand Fund (L.I.Z.); the Burroughs Wellcome Fund (Career Award for Medical Scientists to A.S.N.); and the Starr Cancer Consortium (A.S.N.). L.I.Z. is a Howard Hughes Medical Institute Investigator. **Author contributions:** Bioinformatic analysis: S.Y., C.La., A.S.N., C.P.R.; Conceptualization: C.P.R., L.I.Z.; Funding acquisition: C.P.R., L.I.Z.; Methodology: C.P.R., J.M.C., C.M., J.W.K., C.A., C.Li.; Project administration: C.P.R.; Supervision: C.P.R., L.I.Z.; Visualization: C.P.R.; Writing – original draft: C.P.R.; Writing – review & editing: C.P.R., J.M.C., S.Y., C.M., J.W.K., C.La., A.S.N., C.A., C.Li., L.I.Z. **Competing interests:** L.I.Z. is a founder and stockholder of Fate Therapeutics, CAMP4Therapeutics, and Scholar Rock. C.P.R. and L.I.Z. hold the patent: "Surface calr chemical inducers" (US Patent WO2023244470A1). The remaining authors declare no competing interests. **Data and materials availability:** All data are available in the main text or the supplementary materials. There are no restrictions on sharing reagents used in the study. The RNAseq data were deposited at Sequence Read Archive (SRA) under the following submission numbers: SRR28470429, SRR28470426, SRR28470427, SRR28470424, SRR28470428, and SRR28470425 (PRJNA1092543).

SUPPLEMENTARY MATERIALS

science.org/doi/10.1126/science.adn1629
Figs. S1 to S5
Data S1 to S3
Movie S1 to S8
MDAR Reproducibility Checklist

Submitted 26 November 2023; resubmitted 9 April 2024
Accepted 4 July 2024
10.1126/science.adn1629